Cleaner Engineering and Technology 25 (2025) 100908

Contents lists available at ScienceDirect

Cleaner Engineering and Technology

journal homepage: www.sciencedirect.com/journal/cleaner-engineering-and-technology

Study on the transient thermo-mechanical coupling mechanism at tool-chip interface in ultrasonic vibration assisted chip formation process under sustainable dry machining conditions

Xuelin Chen [a,b], Wen Shao [b,*], Jinyuan Tang [b], Yuansheng Zhou [b], Dimitrios Kontziampasis [c,d,g], Shuai Mo [e], Bo Hu [b,f]

[a] School of Mechanical and Electrical Engineering, Central South University of Forestry and Technology, Changsha, 410004, China
[b] State Key Laboratory of Precision Manufacturing for Extreme Service Performance, College of Mechanical and Electrical Engineering, Central South University, Changsha, Hunan, 410083, China
[c] School of Science and Engineering, University of Dundee, Dundee, DD1 4HN, UK
[d] Dundee International Institute of Central South University, Central South University, Changsha, Hunan, 410013, China
[e] School of Mechanical Engineering, Guangxi University, Nanning, 530004, China
[f] School of Engineering, University of Edinburgh, Edinburgh, EH9 3JW, UK
[g] School of Mechanical Engineering, Faculty of Science and Engineering, The University of Leeds, Leeds, Yorkshire, LS2 9JT, UK

ARTICLE INFO

Keywords:
Sustainable ultrasonic vibration assisted dry machining
Tool-chip interface
Transient thermomechanical characteristics
Cutting mechanism

ABSTRACT

Dry machining has become one of the most promising and sustainable manufacturing processes in mechanical machining. One of the main puzzles for industrial applications of dry machining is tool wear, which are closely related with the transient thermomechanical characteristics of tool-chip interface (TCI). Simultaneously, those characteristics at micro scale can provided the critical insight of cutting mechanics and tool wear in ultrasonic vibration assisted cutting (UVC). However, reports in literature appear to be scarce. In this study the transient model of thermomechanical behavior in TCI is proposed, with a consideration of characteristics changes induced by ultrasonic vibration, as well as a focus on the transient cutting mechanism, as well as stress and friction. The proposed model is validated by comparison with the experimental and published analytical results. Obtained results from the proposed model indicate that the distribution of normal stress and average shear stress are similar to those that are predicted by Zorev's model. However, a noticeable apparent discrepancy appears between the two models regarding the distribution of shear stress. Apparently, the ultrasonic vibration changes the friction via alternating normal and shear stresses, and delays the time for the cutting force and the stress to reach their peak point. Additionally, it is confirmed that the fluctuation and increment of friction coefficient is due to the cutting force reduction in UVC under sustainable dry conditions.

1. Introduction

Dry machining is a sustainable technique, which can satisfy the industries pursuit of low carbon emissions and energy consumption, because of it would avoid the negative effect on environment and health completely, and reduce energy consumption (Goindi and Sarkar, 2017; Fernandes et al., 2020). Tool wear is one of the main puzzles for industrial applications of dry machining. And tool wear is closed related with the transient thermomechanical characteristics of tool-chip interface (TCI), which could not be measured directly in metal cutting (Kesriklioglu et al., 2019). Nowadays, machining cutting with the assistance of ultrasonic vibration has received special attention, as it has been proven that it can reduce the force and temperature that are necessary for cutting. Simultaneously, it can improve the cutting performance, i.e. decrease the tool wear, promotes grain refinement, and vastly improve the surface topography (Gu et al., 2023; Zhang et al., 2024), which are closed related with contact fatigue life (Li et al., 2024; Lv et al., 2025). Ultrasonic vibration has been applied in cutting systems with the purpose of minimizing tissue adhesion and thermal injury (Yao et al., 2021) and enhances the machinability of titanium alloys (Liu et al., 2021; Tan et al., 2020; Zhu et al., 2025), such as longitudinal-bending hybrid ultrasonic vibration-assisted milling (Hu

* Corresponding author.
E-mail address: wen.shao@csu.edu.cn (W. Shao).

https://doi.org/10.1016/j.clet.2025.100908
Received 22 September 2024; Received in revised form 17 January 2025; Accepted 5 February 2025
Available online 7 February 2025

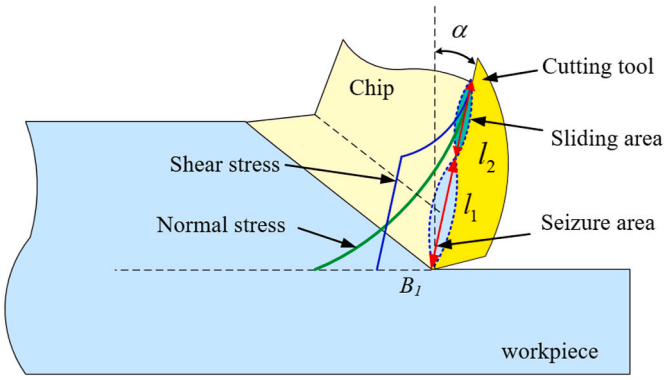

Fig. 1. Schematic representation of Zorev's Model, showing shear stress and normal stress in tool-chip interface.

et al., 2022), two-bending hybrid ultrasonic vibration-assisted milling (Sun et al., 2025), longitudinal-torsional ultrasonic cryogenic cooling drilling system (Shi et al., 2024).

Metal cutting is another chip formation process, in which more than 50% of the cutting energy is consumed for overcoming the friction at TCI (Astakhov, 2006). A considerable amount of effort can be spotted in literature regarding the thermomechanical behavior of tool-chip interfaces. Research has attributed the reduced cutting force and its fluctuations to the reduction of friction force in tool-chip interfaces (Skelton, 1969). Additionally, during the separation between a tool and a chip, which is called "intermitted cutting", the chip acceleration and burnishing effects are also the reasons for the cutting force reduction (Zhang et al., 2018; Nategh et al., 2012). Ultrasonic vibration assisted cutting offers the advantage of promoting the material removal, by the alternating transient characteristics. These are shear angle, deformation mechanism, etc. Ultrasonic softening, which is the recorded change of material strength resulting from ultrasonic also contributes to the force reduction (Chen et al., 2022). As for those different mechanism for the enhancement of cutting performance with the presence of ultrasonic vibration, the analysis of transient thermo-mechanical coupling mechanism at TCI would promote the in-depth understanding of tool wear mechanism and industrial applications of dry machining enhanced by ultrasonic vibration.

1.1. The characteristics of the tool-chip interface in metal cutting

The investigation of the tool-chip interface has been a foundational area of research in metal cutting, with Zorev (1963) recognized as pioneers in the field. He proposed that it was more reasonable to consider the tool-chip interface as a sliding area and a seizure area since the sliding would not happen in the seizure area, which is also supported by Wallace and Boothroyd (1964). A classic model developed for the shear and normal stresses is depicted in Fig. 1. This model is widely applied in metal cutting. Wright (1981) observed that the primary atomic bonds established at the interface resulted in the seizure contact. Doyle et al. (1979) found the seizure area that formed near the cutting edge does not get affected by the lubricant. Bailey and Boothroyd (1968) claimed that the frictional force at the seizure region occupied approximately 90% of the total frictional force. In this named seizure region, huge compressive stress exists, resulting in elevated interfacial temperature and large energy dissipation rate in the chip formation process (Jackson and Wright, 1982). These are the main cause of the rapid wear of cutting tool, while it also affects the shear angle, and tool-chip contact length (Chen et al., 2021a). The seizure area, along with and characteristics of the tool-chip interface exert enormous functions on the chip formation and the tool wear. In parallel, the transient thermomechanical behavior of the tool-chip interface poses as the key for the in-depth understanding of how one can improve cutting performance with ultrasonic vibration and surface characterization (Ni et al., 2019).

1.2. The thermomechanical properties of the tool-chip interface in UVC

Other work has focused on the thermomechanical properties of the tool-chip interface under ultrasonic vibration. Wright et al. (1979) discovered that the tool vibration was responsible for the change in the proportion of seizure, in sliding micro regions, without managing to identify the underlying mechanism. Chou (1994) observed that the friction in seizure area reduced, while the chip movement accelerated with the assistance of ultrasonic vibration. Jamshidi and Nategh (2013) proposed empirical correlations between contact length and normal stress. They calculated the cutting force based on the frictional characteristics of the tool-chip interface, concluding that a larger reduction of normal force than that of the frictional force contributed to the decrease of cutting force. Kumabe et al. (1989) noticed that when the cutting velocity goes beyond the critical cutting velocity, the UVC process becomes useless. Simultaneously, Lotfi and Amini (2018) revealed that when ultrasonic vibration was applied, the temperature in the primary deformation zone increased, while a significant reduction in temperature was observed in the tool-chip contact zone in machining of AISI 304 stainless steel. This temperature variation notably influenced the length of the sticky region. Lotfi et al. (2019) observed that the intermittent contact of the vibrating tool effectively reduces the thermal conduction time at the tool-chip interface, significantly lowering the friction coefficient and contact length, particularly in the sticky region. Lofti et al. (2020) concluded that the cutting force reduction in UVC of Ti6Al4V was due to decreased friction in the TCI. Ni et al. (2018) claim that the ultrasonic vibration elevates the chip size with uniform texture, while the vibration plays a dramatic role on the chip deformation. The shear band was observed by Gao and Jin (2019) as appearing when the ultrasonic vibration was imposed in tangential direction as certain cutting velocity. They performed a series of simulations for the chip flow model, where they spotted that the temperature in shear zone decreases significantly when ultrasonic vibration is present, also attributing to it the disappearance of the shear band. Research by Zarchi et al. (2013) observed that the temperature rises are decreased when ultrasonic vibration is present in cutting, while Doan et al. (2021) noticed the higher temperature in machining of high-entropy alloys under elliptical vibration. Airao and Nirala (2022) observed that the ultrasonic vibration does not always increase the contact length of tool-chip in cutting of SS 304 steel. They documented that the shear angle rises with the enlargement of amplitude and vibrational frequency. The tool-chip contact length increases in analogous fashion with feed rate, while it slightly reduces with the increase of cutting speed. Reduced deformation of shear band when ultrasonic vibration appeared was observed by Patil et al. (2014), while Arefin et al. (2021) defended that the strain hardening and elastic recovery in the intermittent cutting were causes for the decrease of secondary deformation in UVC. Simultaneously, Khajehzadeh and Razfar (2016) studied the average tool temperature with Al2O3-coated tools and found that ultrasonic-assisted turning does not always reduce the average cutting temperature. Zhang et al. (2024) found that the temperature and strain at the tool-chip interface during ultrasonic elliptical vibration-assisted cutting (UEVC) are significantly higher than in conventional cutting processes. This is primarily due to the high-frequency impact of the tool on the chip and the dominant shear frictional forces between the tool and the chip. Dutta and Bartarya (2024) observed that when ultrasonic vibration was applied, the average contact pressure between the tool and chip decreased in machining of AISI D3 steel. The friction coefficient and the temperature in the machining zone also increased with the higher vibration amplitude. The ultrasonic vibration though considerably effects the cutting temperature. And the temperature in cutting zone appeared to never be steady, as it fluctuated during the chip segmentation process (Chen et al., 2021b). This resulted in the birth of complex deformations and led to transient characteristics in UVC. It is essential to note the outmost

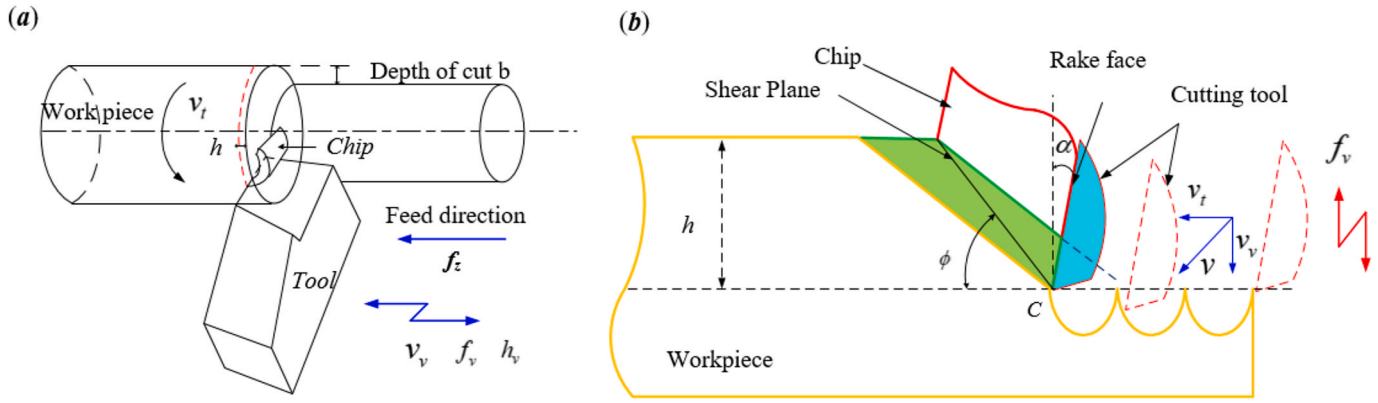

Fig. 2. Schematic diagram of ultrasonic vibration-assisted (a) turning, (b) orthogonal cutting (Chen et al., 2022).

importance of the transient thermomechanical phenomenon of tool-chip interface in chip segmentation process as it allows for the understanding of the mechanism of cutting performance improvement, a fact that underpins and promotes the application of UVC technology.

In the present investigation, a model of transient thermomechanical characteristic of tool-chip interface in UVC is developed. The model takes into account the transient characteristics, i.e. shear angle, flowing stress, as well as transient tool-chip contact length in chip formation process. Subsequently, a validation through a direct comparison is performed between the proposed model's predicted results, experimental results, and published analytical results. The cutting force, friction coefficients, normal and shear stresses at the tool-chip interface, and their corresponding time-varying values are studied. All the above are systematically summarized and discussed in the final section through the lens of their novel contributions on the thermomechanical behavior at the TCI, as well as the cutting force reduction.

2. Principles of cutting mechanisms in UVC

Based on the mechanics of orthogonal cutting and turning (Chen et al., 2021a), the variance of feed rate f_z in turning introduced by ultrasonic vibration are equaled with that of the uncut chip thickness h. Research (Zhang et al., 2018; Kumabe et al., 1989) has shown that the separation might occur when the feed rate is lower than ultrasonic vibration amplitude. It has been reported that chip transportation and not chip separation occurs when the direction of ultrasonic vibration is consisted with that of feed rate (Chou, 1994). And the coupling influence, i.e. cutting parameters, stress, temperature, and soften effect introduced by ultrasonic vibration are emerged. Therefore, in the current study, the ultrasonic vibration is following the feed direction to investigate the thermomechanical characteristic at the tool-chip interface in UVC.

2.1. Modeling of primary shear zone

According to the approach for the equations in section 2.1 (Chen et al., 2022). There, the parameters in UVC are presented in Eqs. 1–14. Fig. 2 shows the mechanics of turning and orthogonal cutting with assistance of ultrasonic vibration.

According to the schematic diagram of turning and orthogonal cutting (Chen et al., 2021a; Vyas and Shaw, 1999), the depth of cutting b is equivalent to chip width. The feed rate in UVC h_z is derived as

$$h_z = h + h_v \sin(2\pi f_v t + \theta) \tag{1}$$

where f_v, θ, t, h_v are the vibration frequency, the initial phrase shift angle, the time, the vibration amplitude in feed direction. h is the undeformed chip thickness (uncut chip thickness) in conventional cutting.

The conventional cutting velocity v_t, the ultrasonic vibration velocity of cutting tool v_v, and the resultant cutting velocity v are expressed with the following equations.

$$v_t = \pi n D_r \tag{2}$$

$$v_v = 2\pi f_v h_v \cos(2\pi f_v t + \theta) \tag{3}$$

$$v = \sqrt{{v_t}^2 + {v_v}^2} \tag{4}$$

in which D_r is he diameter the workpiece, n is the rotation speed.

The effective rake angle is α_v, the shear angle is ϕ_v, the angle between conventional cutting speed and resultant cutting speed is θ_1 in UVC, and are given by the following equations

$$\theta_1 = \arctan\left(\frac{v_v}{v_t}\right) \tag{5}$$

$$\alpha_v = \alpha + \theta_1 \tag{6}$$

$$\phi_v = \phi + \theta_1 \tag{7}$$

in which ϕ and α are the shear angle and the rake angle, respectively in conventional cutting.

The velocity of the deformed chip V_c, and the moving speed of the shear plane V_s are expressed as follows (Chen et al., 2021a)

$$V_c = \frac{\sin\phi_v}{\cos(\phi_v - \alpha_v)} v \tag{8}$$

$$V_s = \frac{\cos\alpha_v}{\cos(\phi_v - \alpha_v)} v \tag{9}$$

The analytical shear angle in UVC is determined as

$$\phi = \frac{5}{8}\alpha_v + \frac{1}{2}\cos^{-1}\left[\exp\left(-52.5\times10^{-3}\left(\frac{\tau_{s,uv}\sqrt{3}}{100 c_2 \rho}\right)^{0.8}\left(\frac{v h_z \times 10^{-3}}{60\omega}\right)^{0.4}\right)\right] \tag{10}$$

where $\tau_{s,uv}$ is the material flowing stress under ultrasonic vibration. it is equal to the yield strength, which presented in Section 3. α_v is the rake angle which is calculated by equation (6). v is the resultant cutting velocity which is calculated by equation (4). h_z is un-deformed chip depth in ultrasonic vibration, which is model by equation (1).

c_2, ρ and ω are the material specific heat, density and temperature conductivity, respectively (Toropov and Ko, 2007; Kushner, 1982). More detailed verifications can be referred in Chen et al. (2023).

The strain (ε_v), strain rate (ε_v'), thickness (Δd_v)of the shear zone in UVC are formulated by following equations

$$\varepsilon_v = \frac{\cos\alpha_v}{\sin\phi_v \cos(\phi_v - \alpha_v)} \tag{11}$$

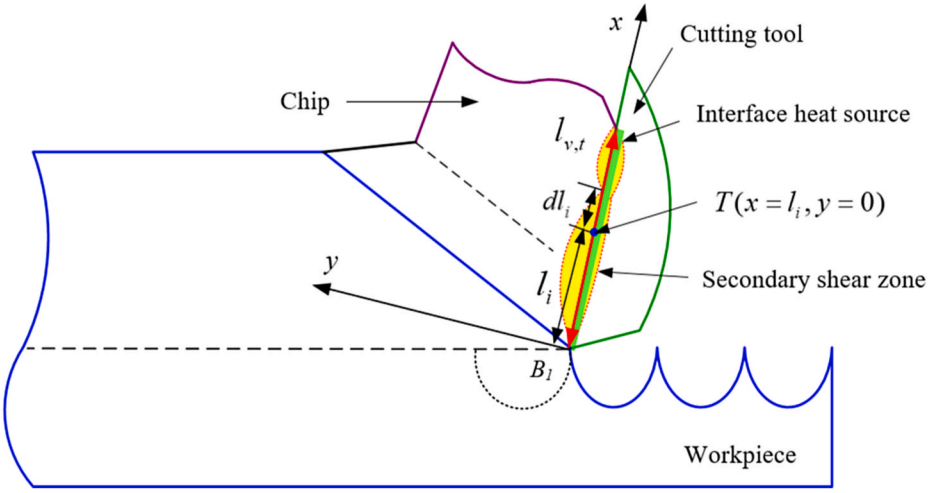

Fig. 3. Schematic representation showing the heat transfer model for the temperature rise at TCI of chip side.

$$\varepsilon_v^{'} = \frac{\nu_v \cos \alpha_v}{\Delta d_v \cos(\phi_v - \alpha_v)} \tag{12}$$

$$\Delta d_v = \frac{h_z}{5.9 \sin \phi_v} \tag{13}$$

Based on the characteristic of the shear region, such as the high temperature and small spatial scale, the diffusion term can be neglected, and the heat transfer equation is simplified with only considering the heat source and thermal convective. The average temperature (T_a) of the shear zone is simplified to

$$T_a = \frac{\varpi \tau_{s,uv} \varepsilon_v^{'}}{\rho c_2 v_v \sin \phi_v} + T_r \tag{14}$$

where ϖ is the Taylor-Quinney coefficient, which is set to 0.85 (Bai et al., 2017).

The plane shear flowing is considering the effect of strain, strain rate, and the heat softening that is introduced by ultrasonic vibration stress, and is

$$\tau_{s,1} = \frac{1}{\sqrt{3}} \left(A + B \left(\frac{\varepsilon_v}{\sqrt{3}} \right)^n \right) \left\{ 1 + m \ln \frac{\varepsilon_v^{'}}{\dot{\varepsilon}_0} \right\} \left\{ 1 - \left(\frac{T_a - T_r}{T_m - T_r} \right)^c \right\} \tag{15}$$

where $\varepsilon_0^{'}$, T_a, T_m and T_r are the reference strain rate, the cutting temperature, melting temperature, and room temperature (300 K), respectively. A, B, C, m, and n are the material constants in Johnson-Cook model (Verma et al., 2018).

Considering the ultrasonic softening effect, the detail derivation procedure of the yield normal stress in UVC is presented in references (Chen et al., 2022). The yield is given as

$$\sigma_{s,uv} = \sigma_s \left(1 - 4\pi^2 f_v^2 \zeta^2 D \rho c\right) \tag{16}$$

where c, σ_s are the speed of ultrasonic wave and the yield strength. D is the ultrasonic softening constant.

The corresponding shear stress is derived as

$$\tau_{s,uv} = \frac{\sigma_{s,uv}}{\sqrt{3}} \tag{17}$$

Accordingly, the stress is given by

$$\tau_{s,uv} = \tau_{s,1} \left(1 - 4\pi^2 f_v^{\,2} \zeta^2 D \rho c\right) \tag{18}$$

According to the principle of minimum energy, the shear angle under ultrasonic vibration is expressed as

$$\phi_v = \frac{\pi}{4} - \frac{\beta_v - \alpha_v}{2} \tag{19}$$

Thus, the friction angle in UVC can be developed as

$$\beta_v = \frac{\pi}{2} - 2\phi_v + \alpha_v \tag{20}$$

Using all the above equations, one can calculate the shear and friction angles in UVC.

The movement in UVC can be considered as the synthesis of traditional cutting and ultrasonic vibration. Therefore, the contact length at any moment can be determined using the empirical model of contact length in conventional cutting.

$$l_{v,t} = h_z \frac{\sin(\phi_v + \beta_v - \alpha_v)}{\sin \phi_v \cos \beta_v} \tag{21}$$

According to the cutting force diagram (Merchant, 1945), the frictional force $F_{\tau,t}$, tangential cutting force $F_{t,t}$, the feed force $F_{f,t}$ and the resultant force F_c can be calculated by follows.

$$F_{\tau,t} = \tau_{s,uv} \frac{h_z}{\sin \phi_v} b \frac{\sin \beta_v}{\cos(\phi_v + \beta_v - \alpha_v)} \tag{22a}$$

$$F_{t,t} = \tau_{s,uv} \frac{h_z}{\sin \phi_v} b \frac{\cos(\beta_v - \alpha_v)}{\cos(\phi_v + \beta_v - \alpha_v)} \tag{22b}$$

$$F_{f,t} = \tau_{s,uv} \frac{h_z}{\sin \phi_v} b \frac{\sin(\beta_v - \alpha_v)}{\cos(\phi_v + \beta_v - \alpha_v)} \tag{22c}$$

$$F_c = \sqrt{F_{t,t}^{\,2} + F_{f,t}^{\,2}} \tag{22c}$$

where b is the depth of cutting, which is equivalent to chip width. For the theoretical cutting forces in x, y, z direction, the corresponded derived procedures can be referenced to Supplied Appendix A (Chen et al., 2022).

2.2. Modeling of tool-chip interface

The stress state of any element that is acting on rake face can be determined by the temperature, the strain, and the strain rate. The temperature at the interface can be determined employing the method of the moving heat source (Jaeger, 1942). Fig. 3 shows the heat transfer model for temperature in tool-chip interface on the chip. Based on the temperature model at the chip side of the TCI (Hou and Komanduri, 1997), the temperature rise at the point $(x = l_i, y = 0)$ of tool-chip contact interface develops as follows.

$$q_{pl} = \frac{F_{\tau,t} V_c}{l_{v,t} b} \tag{23a}$$

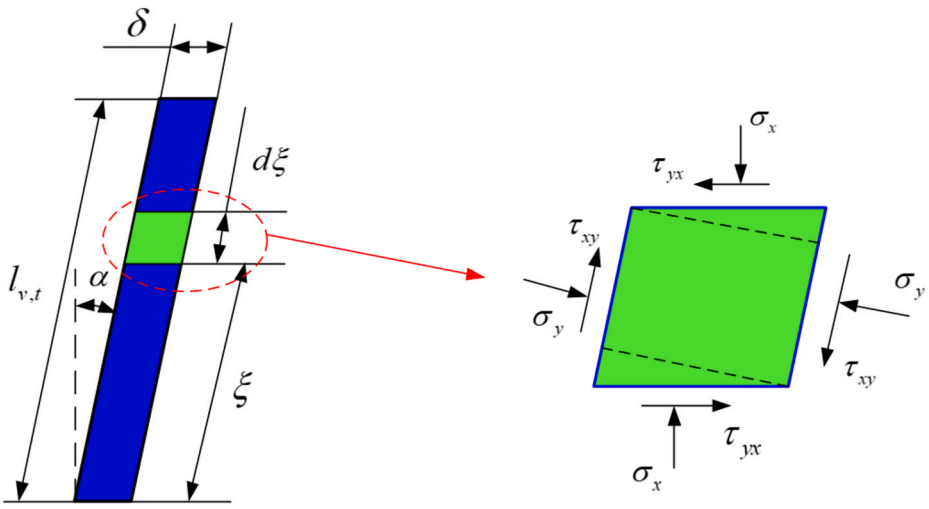

Fig. 4. Schematic representation showing the stress state of the element at the tool-chip contact area.

$$\psi_i = \sqrt{\left(-x + l_{v,t} - l_j\right)^2 + y^2} \tag{23b}$$

$$\psi_i' = \sqrt{\left(-x + l_{v,t} - l_j\right)^2 + (2h_s - y)^2} \tag{23c}$$

$$T_v(x=\xi=l_i, y=0) = \frac{q_{pl}}{\omega\pi}\int_{l_j=0}^{l_{v,t}} e^{-(x-l_j)v/2a}\left[\frac{\psi_i v}{2a} + \frac{\psi_i' v}{2a}\right] dl_j \tag{23d}$$

where q_{pl}, h_s and a are the heat liberation rate per unit area, the deformed chip thickness and the heat diffusivity, respectively.

The deformed chip thickness h_s, and the plastic layer thickness δ on the rake face in UVC are determined as the following equations (Komanduri and Hou, 2001).

$$h_s = \frac{\cos(\phi_v - \alpha_v)}{\sin\phi_v} h_z \tag{24a}$$

$$\delta = 0.1 h_s \tag{24b}$$

According to the shear strain energy yield rule, the formulations of uniaxial flowing stress associated with the plane strain shear flowing stress are expressed as below.

$$\tau = \frac{1}{\sqrt{3}}\sigma \tag{25a}$$

$$\gamma = \sqrt{3}\varepsilon_s \tag{25b}$$

$$\gamma' = \sqrt{3}\varepsilon_s' \tag{25c}$$

The shear stress of workpiece is modeled by the material constitutive Johnson-Cook (J-C) model, which is given by.

$$\tau_s|_{x=\xi,y=0} = \frac{1}{\sqrt{3}}\left(A + B\left(\frac{\gamma|_{x=\xi,y=0}}{\sqrt{3}}\right)^n\right)\left\{1 + m\ln\frac{\gamma'|_{x=\xi,y=0}}{\gamma_0'}\right\}\left\{1 - \left(\frac{T_v|_{x=\xi,y=0} - T_r}{T_m - T_r}\right)^c\right\} \tag{26}$$

where $\gamma|_{x=\xi,y=0}$, $\gamma'|_{x=\xi,y=0}$ and γ_0' are the strain, the strain rate, and the reference strain rate, respectively, for the tool-chip interface at the point $x = l_i, y = 0$ in UVC. $T_v|_{x=\xi,y=0}$ is the temperature at point ($x = \xi, y = 0$) in UVC.

If one considers the ultrasonic softening, the strain, the strain rate that is introduced by ultrasonic vibration, then the shear stress can be determined as.

$$\tau_{s,v}|_{x=\xi,y=0} = \tau_s|_{x=\xi,y=0}\left(1 - 4\pi^2 f^2 \varsigma^2 D\rho c\right) \tag{27}$$

The shear stress of the chip at point ($x = l_i, y = 0$) can be derived from the plastic boundary layer theory (Wright et al., 1979).

$$\tau_{xy}|_{x=\xi,y=0} = \tau_{s-s,v}\left(1 + \frac{c_1 2^{1/3}}{3\left(1 - \frac{c_1}{2}\right)^{1/3}}\left(-\frac{\tau_{s-s,v}\xi}{\mu_{ma} V_c}\right)^{-2/3}\right) \tag{28}$$

where $\tau_{s-s,v}$ is the static shear strength of workpiece under ultrasonic vibration, c_1 is a constant (set as 1.9 in the current work), ξ is the distance between the point of interest and the tool tip, and μ_{ma} is the macroscopic viscosity coefficient (set as 2100 N/m^2) (Chou, 1994; Campbell and Ferguson, 1970).

The static shear stress in condition of ultrasonic vibration is derived as

$$\tau_{s-s,v}|_{x=\xi,y=0} = \tau_{s-s}\left(1 - 4\pi^2\varsigma^2 D\rho c\right) \tag{29}$$

where τ_{s-s} is the static shear strength.

Fig. 4 shows the stress-state in tool-chip interface at chip side. According to the Newton's third law, the normal stress that is acting on the tool-chip interface at the chip side, is equal to the stress that is acting on the rake face. The shear stress under ultrasonic vibration at point ($x = l_i$, $y = 0$) should be equal to material yield strength, which is formulated as.

$$\tau_{xy}|_{x=l_i,y=0} = \tau_{s,v}|_{x=l_i,y=0} \tag{30}$$

Using the formulation between the shear stress and the shear strain, the shear strain γ and the shear modulus G can be derived as follows.

$$\gamma|_{x=\xi,y=0} = \frac{\tau_{xy}}{G}\Big|_{x=\xi,y=0} \tag{31}$$

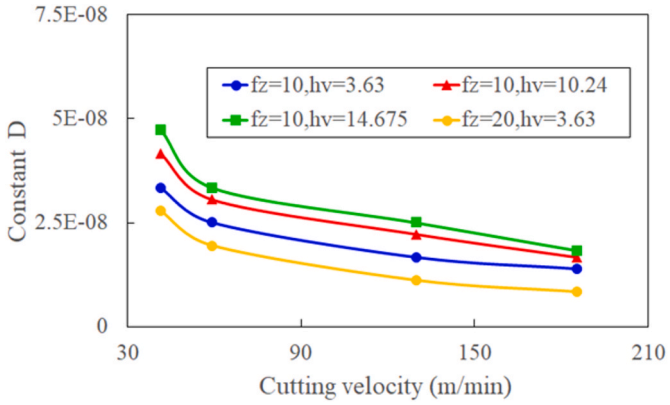

Fig. 5. The varied predicted constant D with the increasing cutting velocity.

$$G=\frac{E}{2(1+\upsilon)} \tag{32}$$

where G and E are the shear modulus and the elastic modulus of the workpiece. υ is Poisson's ratio.

The shear strain $\gamma|_{x=\xi,y=0}$, the shear strain rate $\gamma'|_{x=\xi,y=0}$, and the shear stress τ_{xy} at the point $(x=l_i, y=0)$ can be derived using Eqs. (23)–(32). The deformed length in y direction can be derived from the shear strain and the undeformed chip length.

$$\Delta\delta_y\big|_{x=\xi,y=0}=\gamma|_{x=\xi,y=0}\xi \tag{33}$$

Using to the Bernoulli's principle and equation we estimate the deformed length in x direction is as

$$\Delta\delta_x|_{x=\xi,y=0}=\xi^2\frac{\gamma|_{x=\xi,y=0}}{\delta-\Delta\delta_y|_{x=\xi,y=0}} \tag{34}$$

The normal strains in x and y directions are given by

$$\varepsilon_x|_{x=\xi,y=0}=\xi\frac{\gamma|_{x=\xi,y=0}}{\delta-\xi\gamma|_{x=\xi,y=0}} \tag{35a}$$

$$\varepsilon_y\big|_{x=\xi,y=0}=\frac{\xi}{\delta}\gamma|_{x=\xi,y=0} \tag{35b}$$

The relationship between the linear strain and the normal stress is

$$\varepsilon_x=\frac{1}{E}\left(\sigma_x-\upsilon\sigma_y\right) \tag{36a}$$

$$\varepsilon_y=\frac{1}{E}\left(\sigma_y-\upsilon\sigma_x\right) \tag{36b}$$

Based on the above equations, the normal stresses are determined as

$$\sigma_x=\frac{2\xi}{1-\upsilon}\left(\frac{E}{E\delta-2\tau_{xy}(1+\upsilon)\xi}+\frac{\upsilon}{\delta}\right)\tau_{xy} \tag{37a}$$

$$\sigma_y=\frac{2\xi}{1-\upsilon}\left(\frac{1}{\delta}+\frac{E\upsilon}{E\delta-\tau_{xy}2(1+\upsilon)\xi}\right)\tau_{xy} \tag{37b}$$

The frictional coefficient between the chip and the tool at the interface is

$$\mu_s|_{\xi,t}=\frac{\tau_{xy}}{\sigma_y} \tag{38}$$

The tool-chip contact length including the seizure area and the sliding area is divided into discrete N sections. The observed position at the tool tip is set as $\xi=\frac{n}{N}l_{v,t}, n=1,\cdots,N$. The ultrasonic vibration cycle is discreted into M segments, and accordingly the observed time is $t=\frac{m}{M}f_v$, $m=1,\cdots,M$.

3. Development of an identification method of ultrasonic softening coefficient

As we have shown in our previous study (Chen et al., 2022), the ultrasonic shear stress is

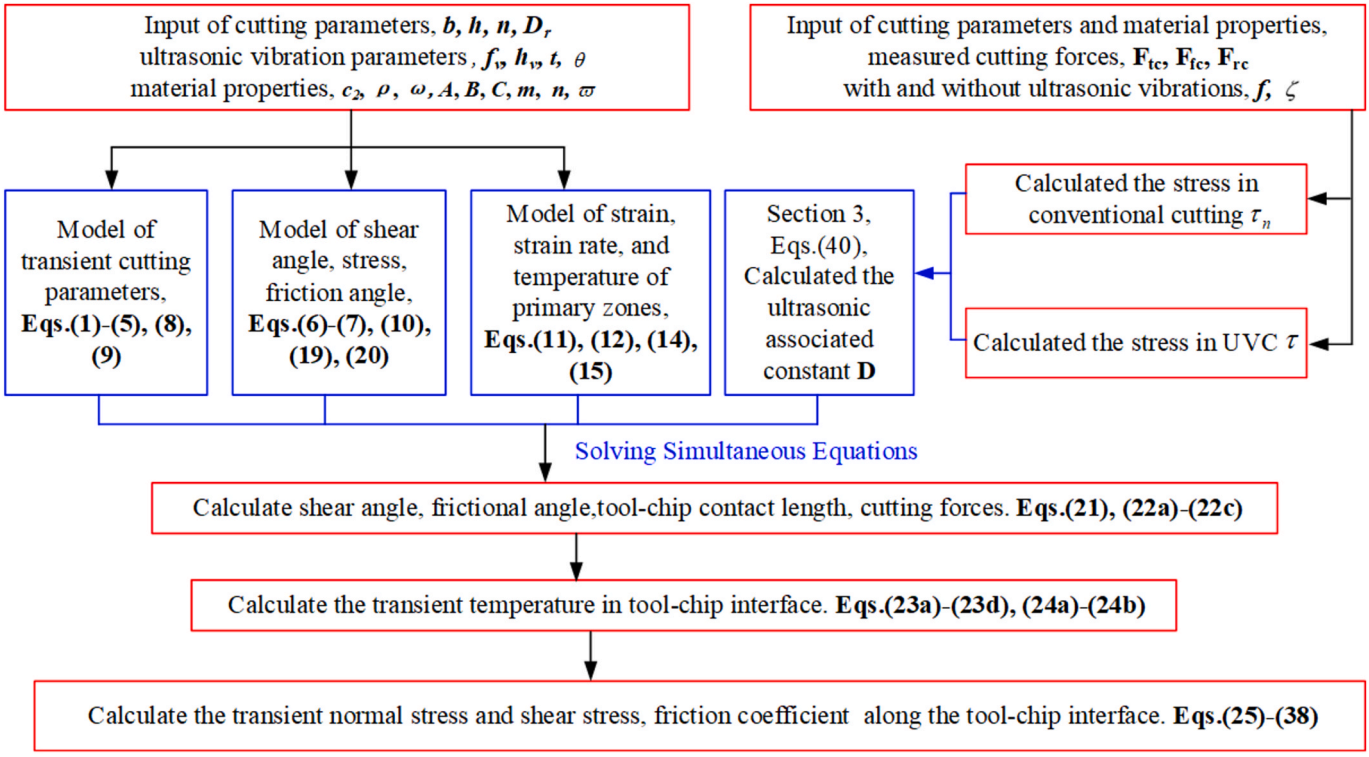

Fig. 6. Process flow showing the input of different cutting forces, showcasing the stress calculation procedure.

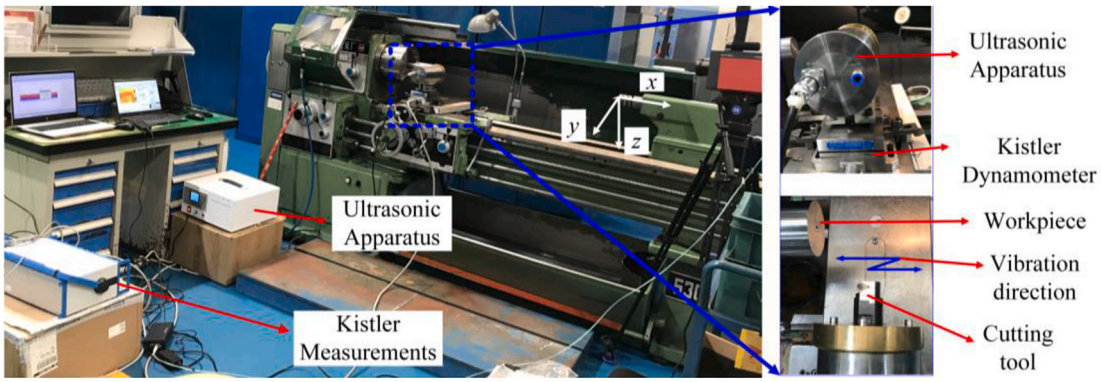

(a)

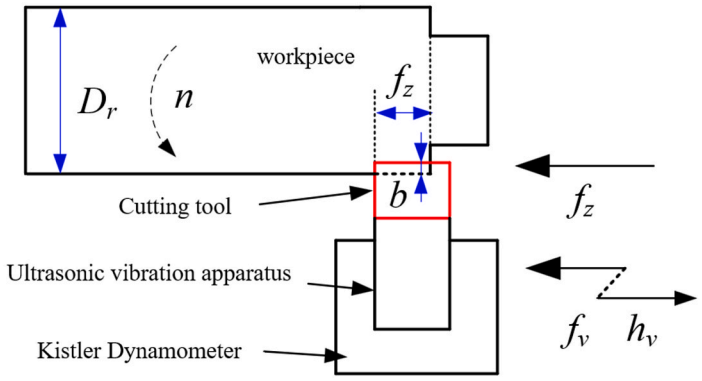

(b)

Fig. 7. Presentation the UVC experiment by: (a) experimental set up and (b) schematic.

Table 1
The Johnson-Cook parameters of the workpiece.

	A	B	m	n	c	$\dot{\varepsilon}_0$	T_m
Ti6Al4V	783	497	0.028	0.28	1	1×10^{-5}	1880K

$$\tau = \frac{\sigma}{\sqrt{3}} = \tau_n\left(1 - 4\pi^2 h_v^2 f_v^2 D\rho c\right) \tag{39}$$

With the input of the shear stress with and without ultrasonic vibration, the constant D can be identified. c is sound speed in workpiece, which varied with temperature. According to the studies on acoustic Properties of VT20 Titanium Alloy proposed by Roshchupkin et al. (2001) and the averaged temperature of shear band, it has been simplified as 3.8×10^3 m/s. The material flowing stress in UVC as well as conventional cutting can be identified with input of cutting force and cutting conditions by the model presented in Supplied Appendix B (Chen et al., 2023). The constant D is calculated and has been presented by Fig. 5. The underlying causes for the trend would be comprehensively analyzed in subsequent research.

Using Eqs. (15) and (16) the ultrasonic softening coefficient can also be calculated. Fig. 6 is a schematic representation of all the necessary calculations and the inputs the procedure for calculating the cutting forces and the stresses.

4. Experimental setup

The UVC experiments under dry conditions are performed using a conventional turning machine. The full experimental apparatus and its schematic diagram are presented in Fig. 7(a) and (b). Fig. 1 also shows

Table 3
Cutting parameters for the machining of Ti6Al4V.

Feed rate per rotation (um) fz h	10
Ultrasonic vibration amplitude (um) h_v	14.675
Spindle speed (rpm) n	112, 160, 350,500
Cutting speed (m/min) v_t	41.5, 59.3, 129.7, 185.26

Table 4
Cutting parameters in UVC experiments.

Feed rate per rotation (um) fz h	10, 20
Ultrasonic vibration amplitude (um) h_v	10.24, 3.63
Spindle speed (rpm) n	112, 240, 350
Cutting speed (m/min) v_t	41.5, 88.9, 129.7

Table 2
The mechanical and thermal attributes of the workpiece (Harzallah et al., 2017; Bai et al., 2017).

Workpiece	Elastic modulus (GPa) E	Poisson's ratio υ	Yield strength (MPa) σ_s	Density (kg/m^3) ρ	Thermal conductivity (W/m.K) ω	Specific heat capacity (J/Kg.k) c_2	Thermal diffusivity (m^2/s) a
Ti6Al4V	105	0.342	880	4430	6.91	520	3×10^{-6}

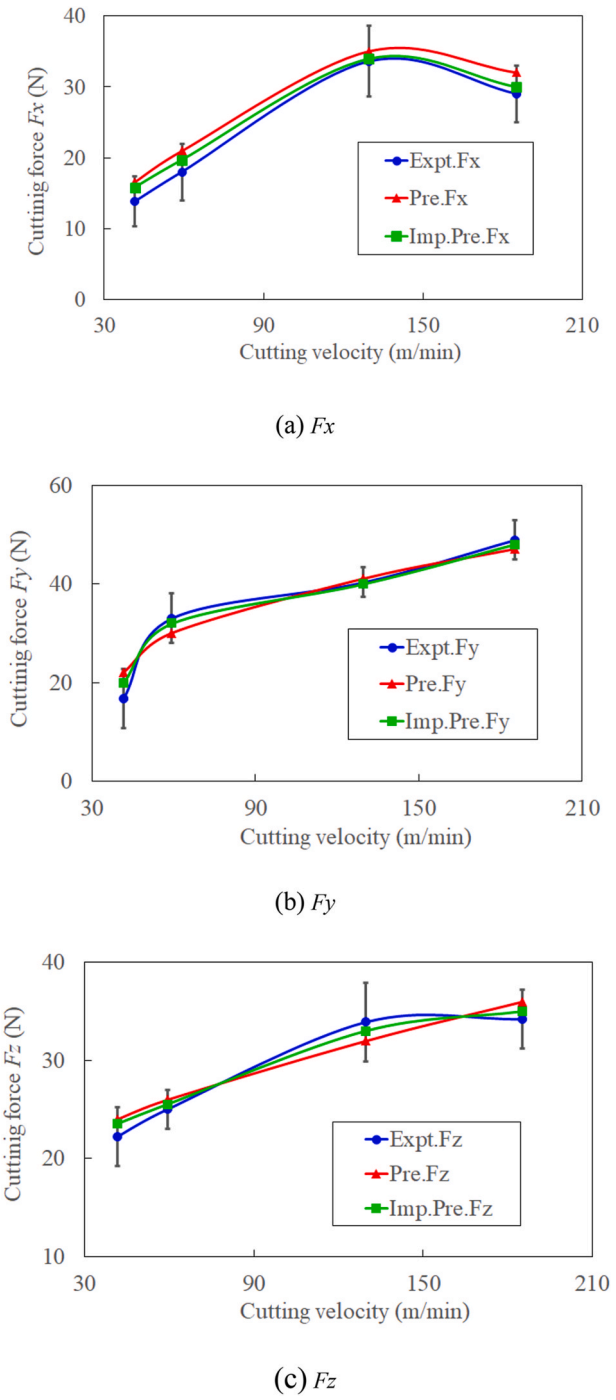

Fig. 8. Comparison between experimental cutting force (Exp.F), initial predictive cutting force (Pre.F), and improved predictive cutting force (Imp.Pre.F in x direction (a) Fx, y direction (b) Fy and z direction (c) Fz. ($hv = 14.675$ μm, $fv = 20{,}283$ Hz, $h = 10$ μm, $b = 0.3$ mm).

the diagram of experiments in which the ultrasonic vibration is added in the feed direction. The cutting force is measured by a Kistler 9257B dynamometer. The cutting tool used for the current experiments consists of PVD-coated TiAlN, and has a rake angle of 0°, along with a cutting edge angle of 60°. A detailed description and corresponding test results can be found in previous work (Chen et al., 2022). The vibration frequency f_v of the ultrasonic equipment is 20,283 Hz. The typical workpiece is a titanium alloy (Ti6Al4V) bar with a diameter of 59 mm. The corresponding J-C, thermal and mechanical attributes of the material are presented in Tables 1 and 2. The cutting depth in the whole experiments is 0.3 mm, the remaining cutting parameters are set and tabulated in Tables 3 and 4.

5. Results and discussion

5.1. Cutting force

The modeling of the primary shear region in the current study (Imp. Pre. Model) is improved by considering ultrasonic softening and its corresponding influences on cutting process compared to the Pre. Model (Chen et al., 2023) (Supplied Appendix C). The average cutting forces are calculated by averaging the integrations of Eq. (23) over time in an ultrasonic vibration cycle. Since the coordinates of the experimental cutting force are different from these of the theoretical cutting force, the latter should be transformed to the experimental measured coordinate, which is presented in Supplied Appendix A.

Fig. 8 shows that the deviations between the predicted and the experimental values decrease when the ultrasonic softening effect is incorporated in ultrasonic vibration assisted machining for Ti6Al4V. The error is presented in Table 5, where the validity and accuracy of the improved model are verified. With the increment of cutting speed, the difference between the predictive cutting forces of the improved model (Imp. Pre. Model) of this study and these predicted by the model in the previous investigation (Pre. Model) increases. The ultrasonic softening effect is reverse analogous to cutting velocity, which is also confirmed by the decrease of the machining force reduction rate. Simultaneously, the strain hardening and heat softening increase analogously with the cutting speed (Arefin et al., 2021; Chen et al., 2021b,c). The plastic recovery and the strain hardening during the reverse moving of the tool decreases with the increase of the cutting velocity. The thermal effect is taken into consideration by incorporating the J-C material model in the proposed model, and it indicates that the ultrasonic softening effect increases analogously with strain hardening. However, the cutting forces are not always reduced when the ultrasonic softening effect is considered. This might be attributed to the varied transient characteristics, as for example ultrasonic softening, thermal softening, and strain hardening that are induced by ultrasonic vibration (Amini et al., 2017). It should be noted that each of the tests is performed using a new cutting tool, and that the test lasts for about 30 s. Additionally, a spirit level equipment is used to ensure the position of cutting tool after the tool renewal in the experiment. It can be seen that the effect of normal abrasion on the deformation of primary shear area is very small. However, it is evident that there is a clear need for more in depth research regarding this fact in order to understand more on the observed behavior.

Table 5
Values of the errors between models 1 and 2, and the averaged experimental values. Model 1 and 2 are equal to model and improved model.

	Fx				*Fy*				*Fz*			
Speed (rpm)	112	160	350	500	112	160	350	500	112	160	350	500
Pre. Model	20%	17%	4%	10%	32%	9%	17%	4%	8%	4%	6%	5%
Imp.Pre. Model	14%	9%	1%	4%	20%	3%	7%	2%	6%	2%	3%	3%

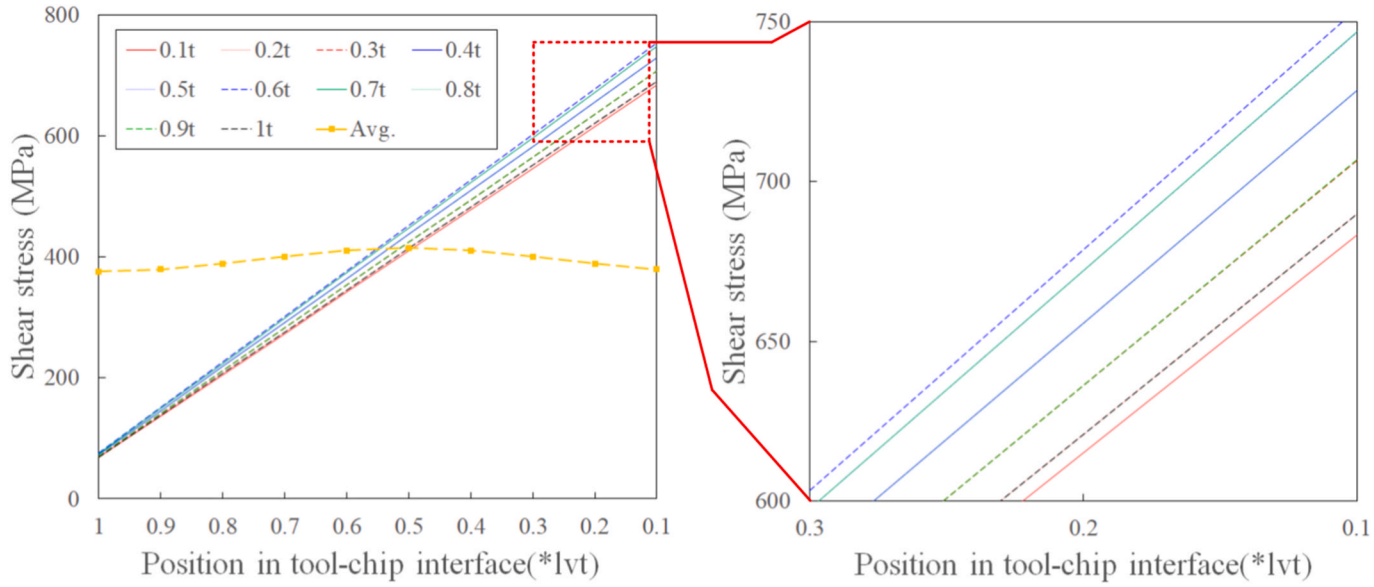

Fig. 9. The variation of shear stress along the TCI. "Avg" represents evolution of averaged the shear stress of entire tool-chip interface with increased tool vibrational stage from 0.1t to t. (n = 112 rpm, h = 10 μm, hv = 3.63 μm).

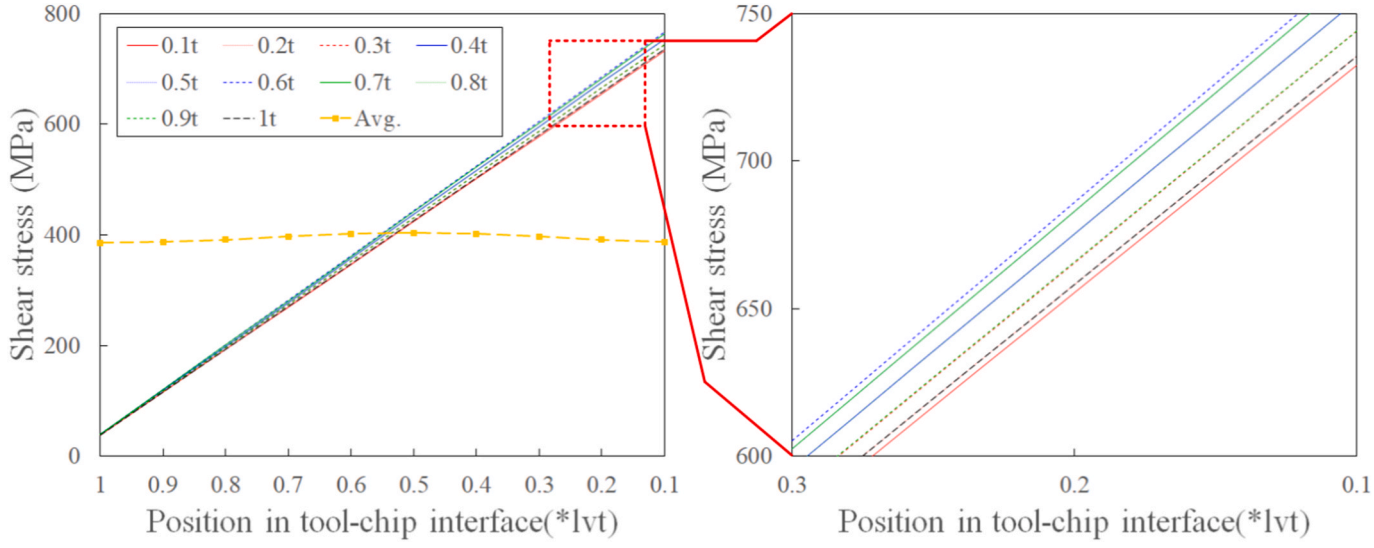

Fig. 10. The variety of shear stress along the TCI (n = 240 rpm, h = 10 μm, hv = 3.63 μm).

5.2. Time varying shear stress along the tool-chip interface

In the following subsections, *t* represents the tool vibration phase that is introduced by the ultrasonic vibration. "Position in tool-chip interface (*lvt)" is defined as the value under the horizontal axis multiplied by the tool-chip contact length. For example, the point of horizontal coordinate is 0.4 in Fig. 8, the mean of "Position in tool-chip interface (*lvt)" is "0.4*lvt" and it shows the tool-chip contact position with the length of 0.4 × *lvt* from the original point. The original point is the tool nose, which is shown in Fig. 3. The variations of shear stress and average shear stress along the tool-chip interface can be seen in Figs. 9–11. The average shear stress is averaged from the stress value of 10 discrete tool-chip contact points at a certain stage of tool vibration. The 10 discrete points are 1*lvt, 0.9*lvt, 0.8*lvt, …, 0.2*lvt, 0.1*lvt, respectively. As can be seen in Fig. 8, the shear stresses increase when the position gradually approaches the tip of the cutting tool. It can also be seen that there is a minor increase of the shear stress within 60% of the chip formation cycle. However, it gradually decreases in the following 40% of the chip formation cycle. The average shear stress along the tool-chip interface with the increase of the chip formation follows a similar trend. In Figs. 9–11, the variation of shear stress in an ultrasonic vibration cycle is shown, which has a reverse analogous relationship with the cutting speed. The variation of shear stress in the chip formation process could certainly benefit from a potential reduction of the cutting force. One can hypothesize that the recovery time for the material deformation that reduces with the rise of cutting velocity, additionally decreases the variation of stress too. This scenario leads to lower fluctuations shown on transient characteristics, as for example the shear angle. These fluctuations contribute to the chip formation process, therefore, the cutting force increases analogously with the cutting speed in UVC. Furthermore, the cutting speed increases the cutting force not only by increasing the deformation, but also via decreasing the variance of shear stress. On the other hand, it has been reported that the elastic recovery reduces with the increase of the cutting velocity (Arefin et al., 2021). In parallel, the variance of the shear stress can originate from the elastic recovery. In the current study, the average shear stress in the total

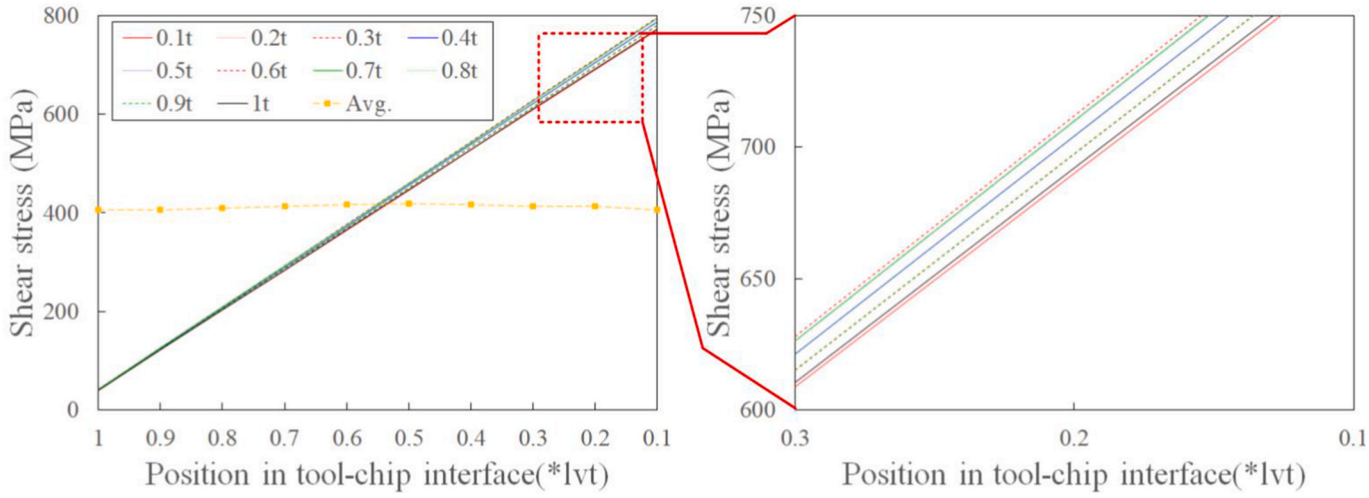

Fig. 11. The variety of shear stress along the TCI (n = 350 rpm, h = 10 μm, hv = 3.63 μm).

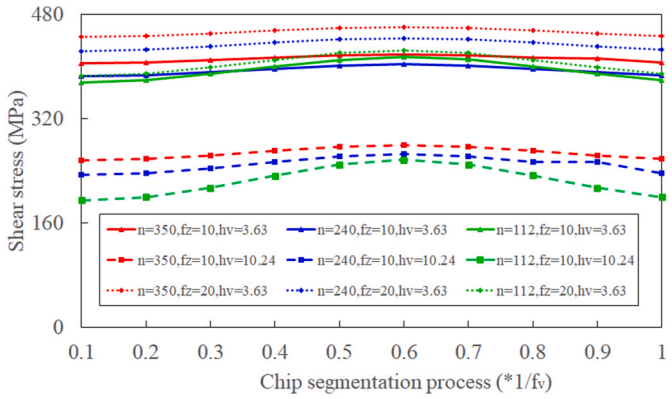

Fig. 12. The variation of average shear stress along TCI in an ultraonic vibration cycle.

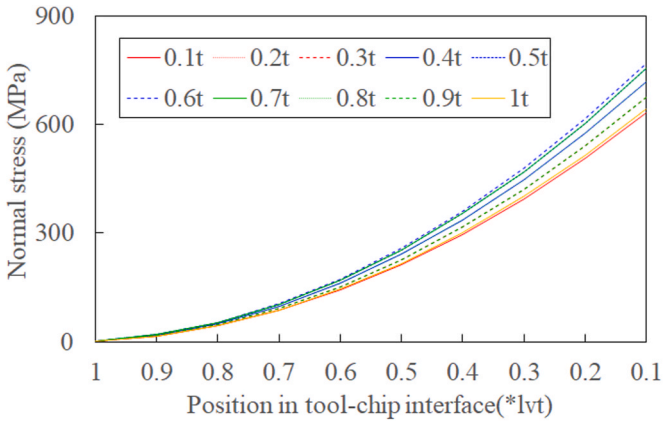

(a) *x* directional normal stress

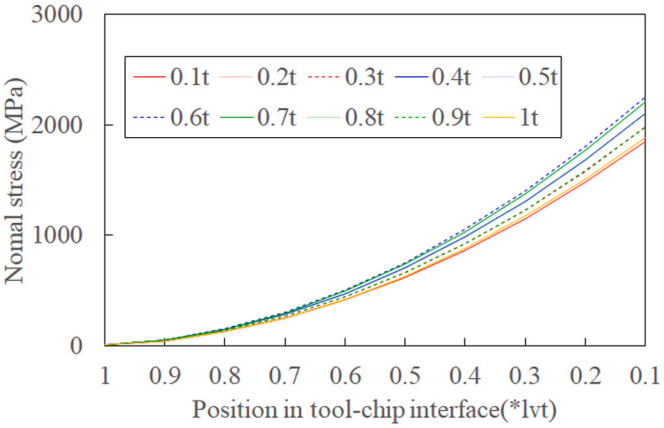

(b) *y* directional normal stress

Fig. 13. Time varying normal stress along the TCI (*n* = 112 rpm, *h* = 10 μm, *hv* = 3.63 μm).

tool-chip contact length is predicted to be approximately 400 MPa, a number that is consistent to the average shear stress of 420 MPa at the seizure area that is obtained from the published model based on the assumption of Zorev friction model (Chen et al., 2023). The shear stress near the tool tip is approximately 800 MPa, similarly to the predicted shear stress from Wright (1981). The change of shear stresses with cutting speed under numerous scenarios follows a similar trend. Fig. 11 shows the average shear flowing stress of the TCI in the chip formation process, under different cutting parameters, in which hv is the vibration amplitude and fz is the feed rate. It is evident that the shear flowing stress increases with feed rate and cutting speed, and rapidly decreases with ultrasonic vibration amplitude. The fluctuation of shear stress in the chip formation process increases with the increase of the ultrasonic vibration amplitude, a fact that is more obvious at low cutting speeds. The normal and shear strain rate increase with the cutting speed and feed rate (Chen et al., 2021a), while also the deformation and thermal softening increase (Dutta et al., 2013.). The reduction of shear stress caused by the introduction of ultrasonic vibration is optimized with the increase of ultrasonic vibration amplitude. When the feed rate is lower than the ultrasonic vibration amplitude, the intermittent cutting mode might be achieved, and cutting force, as well as stress are significantly reduced, as presented in Figss. 9–12. And Fig. 12 also shows that the average shear flowing stress always approaches the maximum value at 60% of the chip formation cycle. It has been reported in literature that the cutting force reaches the peak value at 30% percent of a chip formation cycle in conventional machining of Titanium alloy (Harzallah et al., 2018). The researchers believe that the ultrasonic vibration plays a role and is responsible for the delay of this point, mostly due to the alternation of the transient processing factors, which are incorporated in the proposed model.

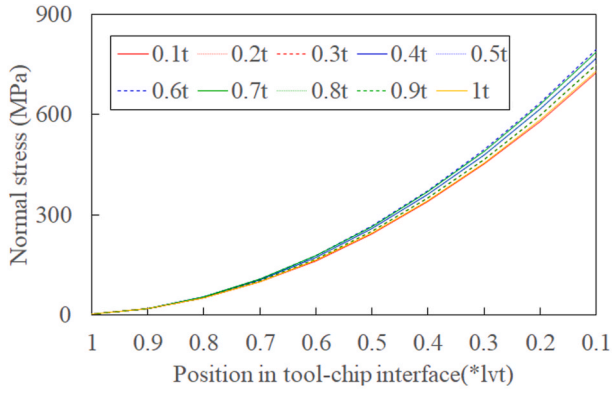

(a) *x* directional normal stress

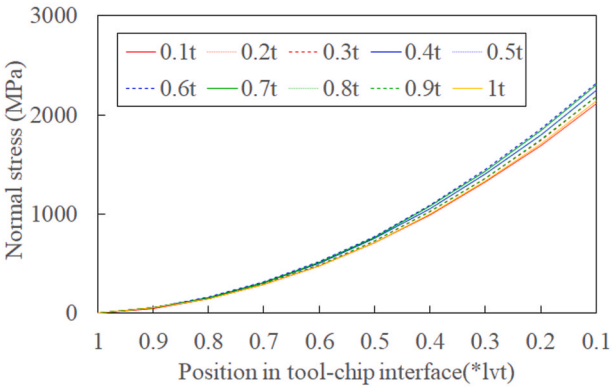

(b) *y* directional normal stress

Fig. 14. Time varying normal stress along the TCI (n = 240 rpm, h = 10 μm, hv = 3.63 μm).

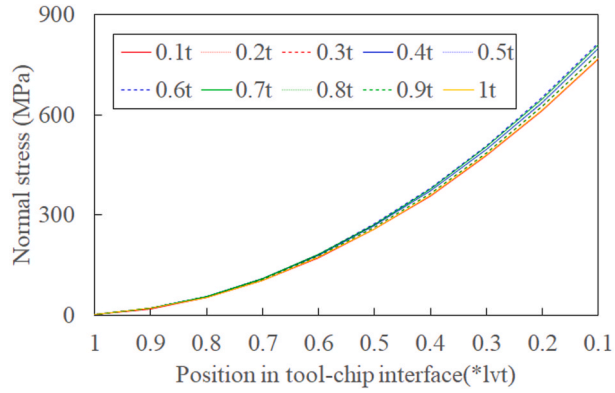

(a) *x* directional normal stress

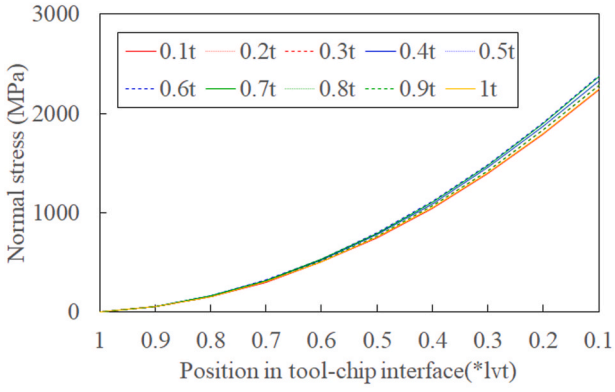

(b) *y* directional normal stress

Fig. 15. Time varying normal stress along the TCI (n = 350 rpm, h = 10 μm, hv = 3.63 μm).

5.3. *Time varying normal stress of tool-chip interface layer*

The variation of the normal stress (σ_x, σ_y) in the plastic layer of the tool-chip interface with different rotation speeds can be seen in Figs. 13–15. There it can be extracted that it increases significantly when the target position moves to the tool tip during the chip formation process. Although the distribution of normal stress is different from the one predicted by Zorev's model, the normal stresses increase exponentially with the decrease of distance from the measured point to the tool tip. This is consistent to what Zorev's model predicts. Similarly to the trend of shear stress, there is a steady increase of normal stress when the value of the chip formation process changes from 0.1t to 0.6t. However, when this value is over 0.6t a sharp decrease of normal stress is observed. The moving of the cutting tool starts reversal and the direction of velocity component at the tool-chip interface is consistent with that of the chip sliding velocity when the time is beyond 0.5t. The critical value is reached after the reversal moving of tool initiates. The deformation and acceleration of the chip still accumulate and there is a point in time where the change of moving direction of the cutting tool affects the cutting process. Additionally, it is known that the cutting force reaches the maximum value and the crack initiates at 30% of the chip formation cycle in conventional cutting (Harzallah et al., 2018). When it comes to 60%, the crack propagation and formation processes is completed (Harzallah et al., 2017). In this work there is a clear indication that the ultrasonic vibration appears to delay the time that the cutting force reaches its peak value. It is also reported in literature, that the temperature reaches its maximum value after the cutting force peaks in chip formation process (Chen et al., 2021b), this shows that also in our case, the temperature is too of great significance for the cutting force reduction.

Compared to the obvious decreased fluctuation of normal stress that is induced by the increase of cutting velocity, the fluctuation of normal stress decreases slightly in conjunction with the feed rate, but it increases rapidly with the increase of the ultrasonic vibration amplitude, as shown in Figs. 16 and 17. The normal stress slightly increases with an increased cutting velocity and feed rate, but increases rapidly with the increase of the ultrasonic vibration amplitude, showing that the acceleration of the chip does not increase with cutting speed. Additionally, literature reports that the deformation in the shear region clearly increases with the increase of cutting speed and feed rate (Chen et al., 2021a), which follows the same trend as the shear stress that is depicted in Fig. 12. The ultrasonic vibration alters the normal stress, resulting in the reduction of the friction between the tool and the chip. This fact is consistent to the published conclusion that the ultrasonic vibration reduces the friction by lowering the normal forces (Skelton, 1969). Regarding flowing stress, the Johnson-Cook model is used for modelling, under the sophisticated state of strain, high strain rate, and temperature. The normal stress in Y direction is much higher than that in the X direction. The normal stress in Y direction is much easier to reach for the strength of the workpiece, and could be the reason why the crack of the chip initiates and propagates in Y direction. The plastic recovery during the reversal moving of the tool decreases with cutting speed (Patil et al., 2014), a fact that is also considered in the J-C material model used in the present study. This is consistent to the trend of the stresses, which initially increases, but then decreases after reaching a critical point. The increased plastic recovery of deformation and the decreased normal stress amplitude with the larger ultrasonic vibration amplitude, all contribute to the increase of fluctuation.

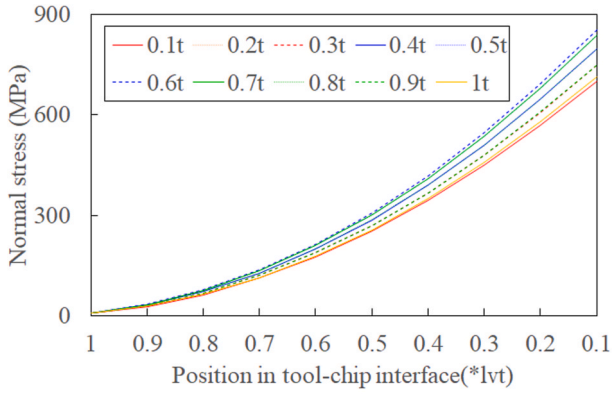

(a) x directional normal stress

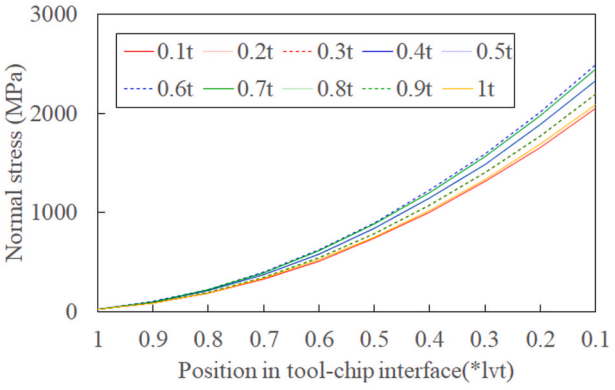

(b) y directional normal stress

Fig. 16. Time varying normal stress along the TCI (n = 112 rpm, h = 20 μm, hv = 3.63 μm).

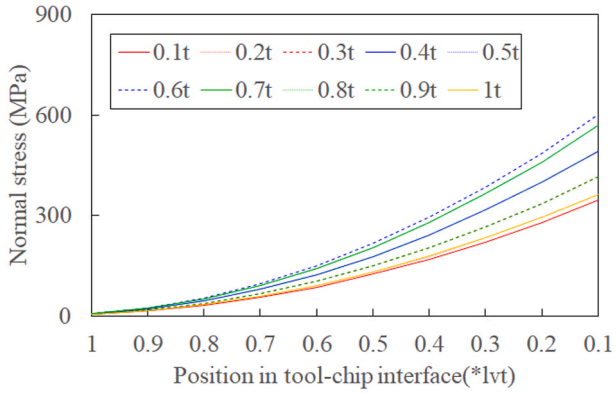

(a) x directional normal stress

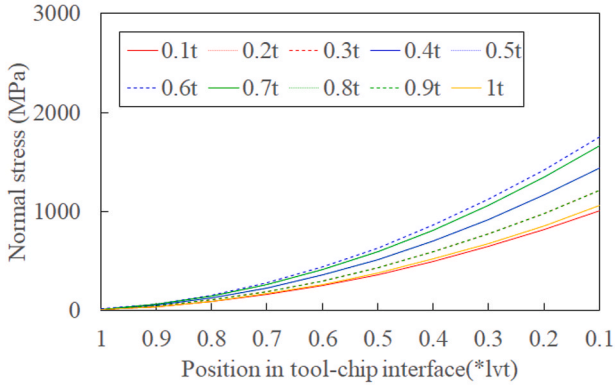

(b) y directional normal stress

Fig. 17. Time varying normal stress along the TCI (n = 112 rpm, h = 20 μm, hv = 10.24 μm).

5.4. *Transient friction coefficient in tool-chip interface*

The variation of friction coefficient along the TCI at the chip formation process is shown in Figs. 18–23. The friction coefficients are calculated by Eq. (38), using the calculated shear and normal stresses. There, it is evident that the frictional coefficient increases slightly when the distance ranges from 0 to 0.7*lvt and increases rapidly when the distance is over 0.7*lvt. The reason behind this behavior is the relatively high increase rate of normal stress, while both the shear and normal stresses are high. There is still material flowing inside the seizure area, although the friction is very low. The deformation of the plastic layer at the TCI can also be indicated by the friction coefficient. When the location nears the tool tip, the material might break by the huge stress, which is dominated by the normal stress. This means that the crack propagates in the direction moving away from the tool tip, a fact that is consistent with the results in literature (Wang et al., 2020.). The schematic diagram of the crack propagation is presented in Fig. 24. There, two crack propagation paths form the crack area. This result is consistent with the SEM photo of the cutting zone shown in Refs. (Chen et al., 2021a; Arefin et al., 2021; Vyas and Shaw, 1999; Amini et al., 2017), which also verify the validity of the model.

The effective cutting velocity is defined as the maximum tangential velocity of ultrasonic vibration in UVC (Jamshidi and Nategh, 2013), and the empirical threshold of the critical cutting speed is proposed based on experimental data published by Wang and Zhao (1987). The critical cutting velocity is 27.74 m/min and the corresponding rotation velocity is 150 rpm. When cutting speed increases, the friction coefficient decreases rapidly before the critical velocity is reached. After that point, the friction coefficient is almost stable. This is consistent to the relative smoother chip morphology in the tool side with smaller friction coefficient and larger cutting speed, as presented SEM micrographs of the chip morphology in tool side when h = 30 μm and fv = 3.63 μm. (a) 350 rpm, (b)240 rpm and (c)112 rpm in Fig. 14 in previous research (Chen et al., 2023). The increased friction force also leads to the decrease of the reduction rate of the machining force. It has also been reported in literature that the ultrasonic vibration lowered the cutting force by decreasing friction in a plethora of (Patil et al., 2014; Arefin et al., 2021). The corresponding average frictional coefficients without ultrasonic vibration that are calculated by the measured cutting force in conventional cutting are 0.85, 0.74, 0.7 for rotation speed of 112 rpm, 240 rpm and 350 rpm, respectively. Compared to the frictional coefficient in UVC presented by Fig. 22, these friction coefficients are in reality lower than the ones in UVC. The coefficient of friction is not necessarily correlated with the intensity of frictional deformation at the tool-chip interface. Instead, the intensity of friction is closely associated with high temperature and high pressure. Therefore, it appears that the ultrasonic vibration alters the friction by changing the values of normal and shear stresses, with these changes causing the cutting force reduction by ultrasonic vibration.

The fluctuation of friction coefficient increases analogously with ultrasonic vibration amplitude and feed rate, as shown in Figs. 20–21. These values decrease rapidly with ultrasonic vibration amplitude and change slightly with feed rate, as shown in Fig. 23. These results indicate that the stress state and the stress ratio between shear stress and normal stress of the TCI also change. The moving of tool might be the main cause of the fluctuation, which fluctuation is significant affected by the feed rate and the ultrasonic vibration amplitude when the cutting velocity is lower than the critical value. The enhanced machining performance that is introduced by the ultrasonic vibration has shown the same dependence. The fluctuation is beneficial to the decrease of cutting force, and

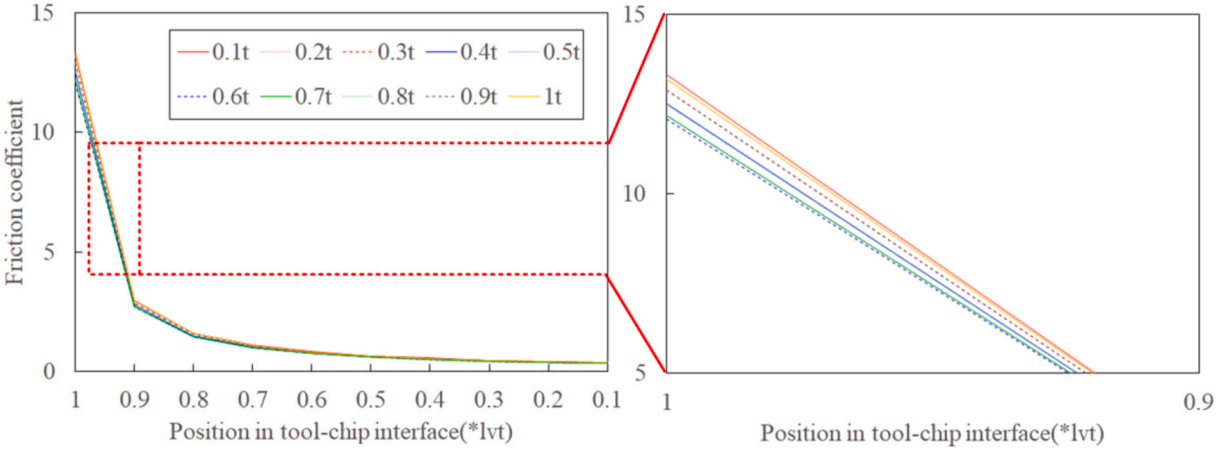

Fig. 18. Time varying friction coefficient (n = 112 rpm, h = 10 μm, hv = 3.63 μm).

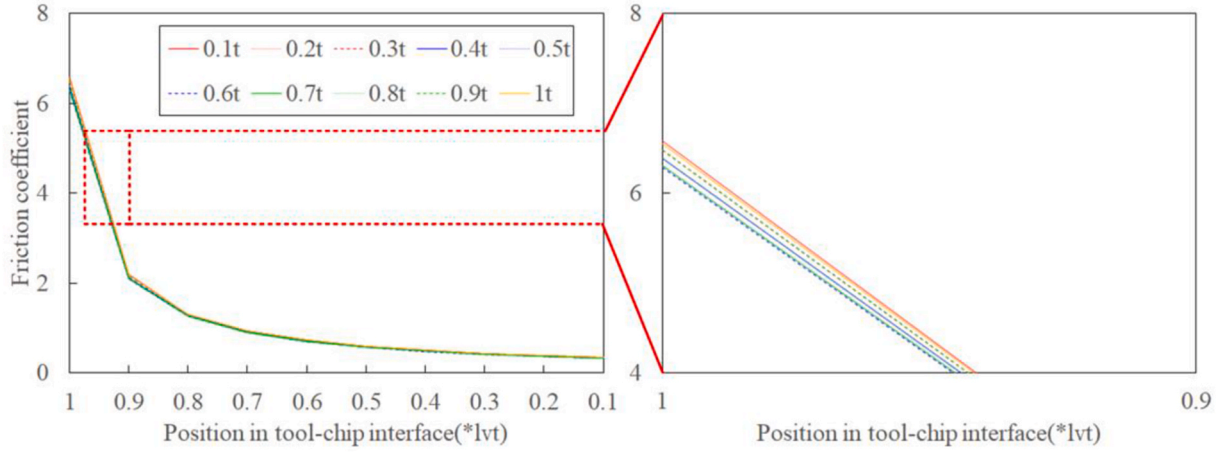

Fig. 19. Time varying friction coefficient (n = 240 rpm, h = 10 μm, hv = 3.63 μm).

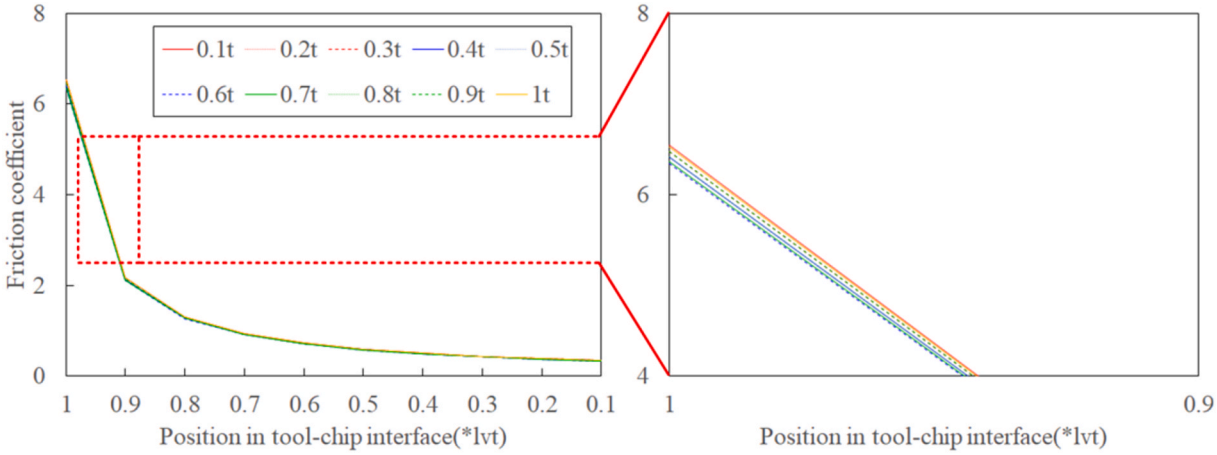

Fig. 20. Time varying friction coefficient (n = 350 rpm, h = 10 μm, hv = 3.63 μm).

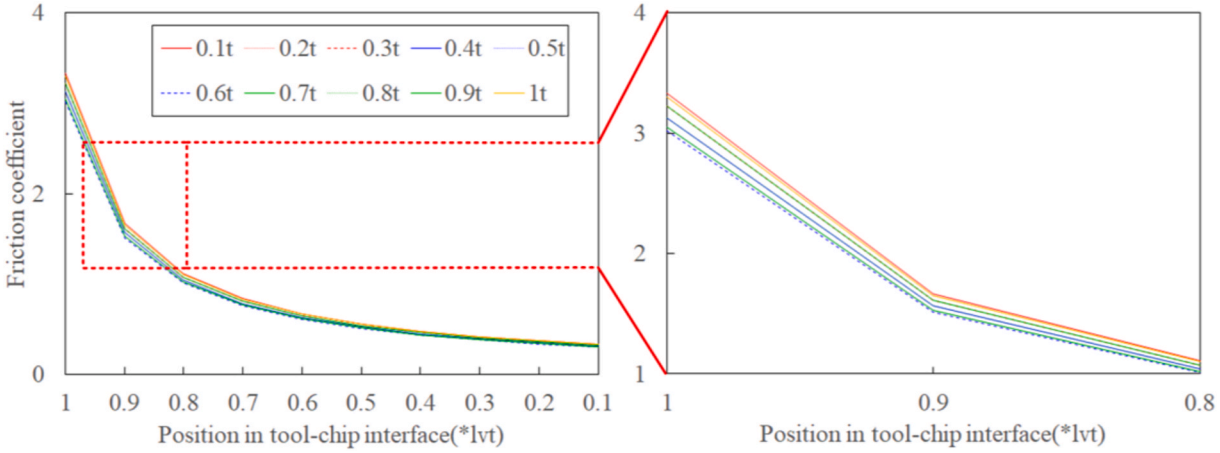

Fig. 21. Time varying friction coefficient (n = 112 rpm, h = 20 μm, hv = 3.63 μm).

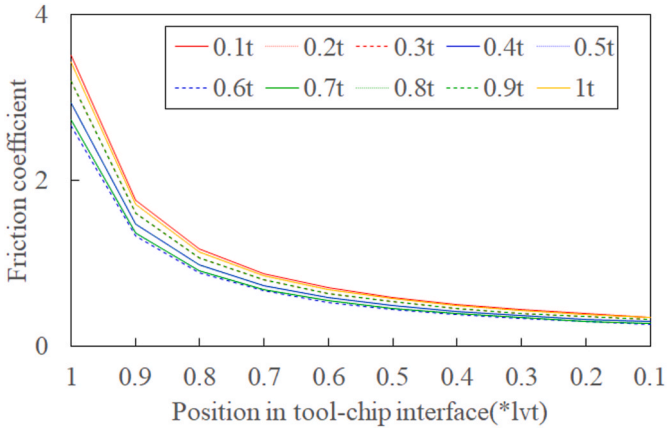

Fig. 22. Time varying friction coefficient (n = 112 rpm, h = 10 μm, hv = 10.24 μm).

the reduction of the cutting force is induced by the fluctuation of the friction coefficient rather than its amplitude.

6. Conclusions

In the present work, the model of transient thermomechanical behavior at the tool-chip interface (TCI) is proposed, taking into consideration the transient cutting mechanism, the temperature, etc.

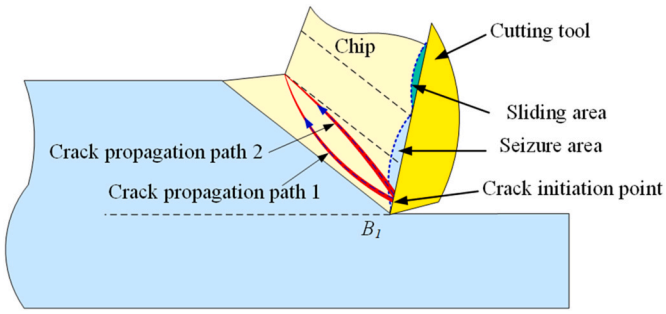

Fig. 24. Schematic diagram of the crack propagation paths in cutting zone, showing the two possible propagation paths, the sliding area, the seizure area, and the crack initiation point.

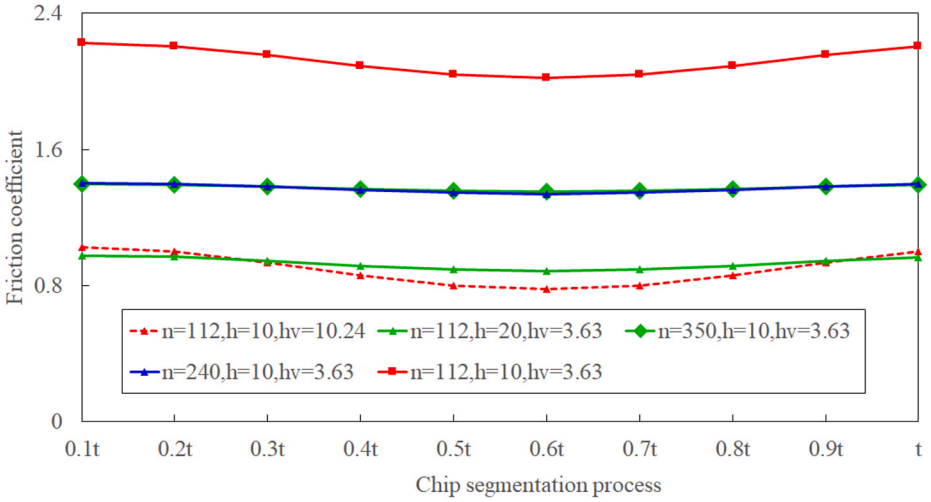

Fig. 23. The average friction coefficient in chip formation process under different cutting parameters.

The proposed model is validated via contrast the predicted, the experimental, with the published analytical results. The main novel insights of the cutting mechanism are summarized as follows.

- ➢ The distribution of shear stress that is predicted by the proposed model is different from that calculate by Zorev's model, a fact that needs clarity and should be further investigated. Additionally, the average shear stress and the distribution of normal stress that is calculated by those two models are close. The current work provides an innovative method for calculating the shear stress and the normal stress at the TCI in UVC.
- ➢ Ultrasonic vibration delays the time for the cutting force and the stress to reach their peak point. This fact lowers the fluctuations of cutting force and also stabilizes the chip formation process.
- ➢ The crack in shear band initiates near the tool tip and propagates away from the tool tip. The propagation is controlled by the normal stress state, as it takes up a major proportion, and also delays the time for the cutting force to reach its peak value.
- ➢ The ultrasonic vibration changes the friction by altering both normal and shear stresses. Moreover, it is confirmed that the ultrasonic vibration increases the value of the friction coefficient and its fluctuation, rather than lowering the value of friction in UVC.

Future work needs to consider and study the effect of the ultrasonic vibration on the adhesion between the tool and the workpiece, as well as the impact of flank surface ironing the machined ridges. The authors have checked the cutting tool and found that the amount of chip adhesion to the cutting tool in UVC appeared to be much less than that in equivalent conventional cutting. Simultaneously, the author would continue to work on solving the cutting force using the transient temperature in the primary shear region, providing the temperature distribution profile of this region in UVC. The author can study the differences in temperature and stress at the tool-chip interface calculated using the transient temperature and the average temperature, along with their distributions. Additionally, the tool wear, residual stress and constant D, chip segmentation frequency in UVC would also be studied. In-depth analysis on those phenomena will allow for the improvement of our understanding of the mechanisms of cutting, leading to better handle sample handling during traditional manufacturing techniques.

CRediT authorship contribution statement

Xuelin Chen: Writing – original draft, Visualization, Formal analysis, Data curation, Conceptualization. **Wen Shao:** Writing – review & editing, Supervision, Project administration, Methodology. **Jinyuan Tang:** Supervision, Investigation, Funding acquisition. **Yuansheng Zhou:** Writing – review & editing, Data curation, Conceptualization. **Dimitrios Kontziampasis:** Writing – review & editing, Conceptualization. **Shuai Mo:** Supervision, Methodology, Conceptualization. **Bo Hu:** Writing – review & editing, Methodology, Conceptualization.

Declaration of competing interest

The authors declare that they have no known competing financial interests or personal relationships that could have appeared to influence the work reported in this paper.

Acknowledgment

This work was supported by National Natural Science Foundation of China [No.52075558], Research Foundation of education Bureau of Hunan province [Grants No. 22B0265], Natural Science Foundation of Hunan province [Grants No. 2024JJ6717, 2021JJ20071], The science and technology innovation Program of Hunan Province [No. 2021RC3012], Hunan Provincial Key R&D Program [No. 2023GK2053], State Key Laboratory of Precision Manufacturing for Extreme Service Performance through [ZZYJKT2019-08] and Central South University Innovation-Driven Research Program [No. 2023CXQD050].

Appendix A. Supplementary data

Supplementary data to this article can be found online at https://doi.org/10.1016/j.clet.2025.100908.

Data availability

Data will be made available on request.

References

Airao, J., Nirala, C.K., 2022. Analytical modeling of machining forces and friction characteristics in ultrasonic assisted turning process. J. Manuf. Sci. E-T ASME 144, 021014. https://doi.org/10.1115/1.4052129.
Amini, S., Lotfi, M., Paktinat, H., Kazemiyoun, M., 2017. Characterization of vibratory turning in cutting zone using a pneumatic quick-stop device. Eng. Sci. Technol. Int. J. 20, 403–410. https://doi.org/10.1016/j.jestch.2017.03.003.
Arefin, S., Zhang, Z., Kumar, A.S., Neo, D.W.K., Wang, Y., 2021. Study of chip formation mechanism in one-dimensional vibration-assisted machining. J. Mater. Process. Technol. 291, 117022. https://doi.org/10.1016/j.jmatprotec.2020.117022.
Astakhov, V.P., 2006. Tribology of Metal Cutting, first ed. Elsevier, London.
Bai, W., Sun, R., Roy, A., Silberschnidt, V., 2017. Improved analytical prediction of chip formation in orthogonal cutting titanium alloy Ti6Al4V. Int. J. Mech. Sci. 133, 357–367. https://doi.org/10.1016/j.ijmecsci.2017.08.054.
Bailey, J., Boothroyd, G., 1968. Critical review of some previous work on the mechanics of the metal-cutting process. J. Eng. Ind. ASME 1, 54–62. https://doi.org/10.1115/1.3604605.
Campbell, J.D., Ferguson, W.G., 1970. The temperature and strain-rate dependence of the shear strength of mild steel. Philos. Mag. 169 (21), 63–82. https://doi.org/10.1080/14786437008238397.
Chen, X., Shao, W., Tang, J., Hu, B., 2023. An investigation on cutting mechanism and thermomechanical behaviors at tool-chip interface in ultrasonic vibration assisted cutting of Ti6Al4V alloy. Int. J. Adv. Manuf. Technol. 129, 3027–3046. https://link.springer.com/article/10.1007/s00170-023-12430-w.
Chen, X., Tang, J., Ding, H., Liu, A., 2021a. A new geometric model of serrated chip formation in high speed machining. J. Manuf. Process. 62, 632–645. https://doi.org/10.1016/j.jmapro.2020.12.053.
Chen, X., Tang, J., Ding, H., Liu, A., 2021b. An accurate transient model for temperature fluctuation on localized shear band in serrated chip formation. Int. J. Mech. Sci. 204, 106588. https://doi.org/10.1016/j.ijmecsci.2021.106588.
Chen, X., Tang, J., Ding, H., Liu, A., 2021c. Experimental study on the evolution of chip morphology, chip formation, and surface topography with cutting parameters, and their relationships in dry milling of cast aluminum alloy with PCD inserter. J. Mech. Sci. Technol. 35 (4), 1651–1662. https://link.springer.com/article/10.1007/s12206-021-0328-3.
Chen, X., Tang, J., Shao, W., Hu, B., Ye, J., 2022. An analytical and experimental study on cutting characteristics and transient cutting force modeling in feed directional ultrasonic vibration-assisted cutting of high strength alloys. Materials 15, 7388. https://doi.org/10.3390/ma15207388.
Chou, C.L., 1994. Wave Effects of Ultrasonic Vibration on Machining. Ph.D. Thesis. The Pennsylvania State University.
Doan, D., Fang, T., Chen, T., 2021. Machining of mechanism and deformation behavior of high-entropy alloy under elliptical vibration cutting. Intermetallics 131, 107079. https://doi.org/10.1016/j.intermet.2020.107079.
Doyle, E.D., Home, J.G., Tabor, D., 1979. Frictional interactions between chip and rake face in continuous chip formation. Proc. Roy. Soc. London Series A366, 173–183. https://doi.org/10.1098/rspa.1979.0046.
Dutta, P., Bartarya, G., 2024. Understanding tool chip interaction through experimental and numerical analysis during vibration assisted turning of AISI D3 steel. P. I. Mech. E. Part C J. Mech. Eng. Sci. 238 (9), 3850–3863.
Dutta, R.K., Petrov, R.H., Delhez, R., Hermans, M.J.M., Richardson, I.M., Böttger, A., Böttger, A.J., 2013. The effect of tensile deformation by in situ ultrasonic treatment on the microstructure of low-carbon steel. Acta Mater. 61 (5), 1592–1602. https://doi.org/10.1016/j.actamat.2012.11.036.
Fernandes, M.E.P., Melo, A.C.Z., oliveira, A.J., Chesman, C., 2020. Hard truning of AISI D6 tool steel under dry, wet and cryogenic conditions: an economic investigation aimed at achieving a sustainable machining approach. Clean. Eng. Technol. 1, 100022. https://doi.org/10.1016/j.clet.2020.100022.
Gao, J., Jin, X., 2019. Effects of ultrasonic vibration assistance on chip formation mechanism in cutting of Ti6Al4V. J. Manuf. Sci. E-T ASME 141, 121007. https://doi.org/10.1115/1.4045129.
Goindi, G.S., Sarkar, P., 2017. Dry machining: a step towards sustainable machining-Challenges and future directions. J. Clean. Prod. 165, 1557–1571. https://doi.org/10.1016/j.jclepro.2017.07.235.
Gu, G.Q., Wu, S.J., Wang, D.Z., Zhou, S., Zhu, L.D., An, Q.L., et al., 2023. A review of the research on the variation of tool's motion trajectory and its influence on the formation mechanism of surface quality in ultrasonic vibration machining. J. Manuf. Process. 107, 294–319. https://doi.org/10.1016/j.jmapro.2023.10.025.

Harzallah, M., Pottier, T., Gilblas, R., Landon, Y., Mousseigne, M., Senatore, J., 2018. A coupled in-situ measurement of temperature and kinematic fields in Ti6Al4V serrated chip formation at microsacle. Int. J. Mach. Tool Manufact. 130–131, 20–35. https://doi.org/10.1016/j.ijmachtools.2018.03.003.

Harzallah, M., Pottier, T., Senatore, J., Mousseigne, M., Germain, G., Landon, Y., 2017. Numerical and experimental investigations of Ti-6Al-4V chip generation and thermo-mechanical couplings in orthogonal cutting. Int. J. Mech. Sci. 134, 189–202. https://doi.org/10.1016/j.ijmecsci.2017.10.017.

Hou, Z.B., Komanduri, R., 1997. Modeling of thermomechanical shear instability in machining. Int. J. Mech. Sci. 39, 273–1314. https://doi.org/10.1016/S0020-7403(97)00017-9.

Hu, W., Du, P., Qiu, X., Zhao, X., Hu, Z., Zhang, J., Liu, Y., 2022. Enhanced dry machinability of TC4 Titanium alloy by longitudinal-bending hybrid ultrasonic vibration-assisted milling. J. Clean. Prod. 379, 134866. https://doi.org/10.1016/j.jclepro.2022.134866.

Jackson, P.S., Wright, P.K., 1982. Application of plastic boundary layer theory to metal machining. J. Eng. Ind. ASME. 1, 358–362. https://doi.org/10.1115/1.3185842.

Jaeger, J.C., 1942. Moving source of heat and temperature at the sliding contact. P. Roy. Soc. NSW 76, 203–224. https://doi.org/10.5962/p.360338.

Jamshidi, H., Nategh, M.J., 2013. Theoretical and experimental investigation of the frictional behavior of tool-chip interface in ultrasonic-vibration assisted turning. Int. J. Mach. tools Manuf. 65, 1–7. https://doi.org/10.1016/j.ijmachtools.2012.09.004.

Kesriklioglu, S., Arthur, C., Morrow, J.D., Pfefferkorn, F.E., 2019. Characterization of tool-chip interface temperature measurement with thermocouple fabricated directly on the rake face. J. Manuf. Sci. E-T ASME. 141, 091008. https://doi.org/10.1115/1.4044035.

Khajehzadeh, M., Razfar, M.R., 2016. Theoretical modeling of tool mean temperature during ultrasonically assisted turning. P. I. Mech. E. Part B J. Eng. Manuf. 230 (4), 675–693.

Komanduri, R., Hou, Z.B., 2001. Thermal model of the metal cutting process: part 2-temperature rise distribution due to frictional heat source at the tool-chip interface. Int. J. Mech. Sci. 43, 55–78. https://doi.org/10.1016/S0020-7403(99)00104-6.

Kumabe, J., Fuchizawa, K., Soutome, T., Nishmoto, Y., 1989. Ultrasonic superposition vibration cutting of ceramics. Precis. Eng. 1, 71–77. https://doi.org/10.1016/0141-6359(89)90055-X.

Kushner, V.S., 1982. Thermo-Mechanical Theory of Continuous Cutting of Plastic Metals. Irkutsk University Press, Irkutsk (in Russian).

Li, X., Shao, W., Tang, J., Ding, H., You, S., Zhao, J., et al., 2024. Numerical modeling and experimental investigation on fatigue failure and contact fatigue life forecasting for 8620H gear. Eng. Fract. Mech. 296, 109861. https://doi.org/10.1016/j.engfracmech.2024.109861.

Liu, Y., Geng, D., Shao, Z., Zhou, Z., Jiang, X., Zhang, D., 2021. A study on strengthening and machining integrated ultrasonic peening drilling of Ti6Al4V. Mater. Des. 212, 110238. https://doi.org/10.1016/j.matdes.2021.110238.

Lofti, M., Amini, S., Akbari, J., 2020. Surface integrity and microstructure changes in 3D elliptical ultrasonic assisted turning of Ti6Al4V: FEM and experimental examination. Tribol. Int. 151, 106492. https://doi.org/10.1016/j.triboint.2020.106492.

Lotfi, M., Amini, S., 2018. Effect of ultrasonic vibration on frictional behavior of tool-chip interface: finite element analysis and experimental study. P. I. Mech. E. Part B J. Eng. Manuf. 232 (7), 1212–1220.

Lotfi, M., Amini, S., Ashrafi, H., 2019. Theoretical and numerical modeling of tool-chip friction in ultrasonic-assisted turning. P. I. Mech. E. Part E J. Pro. Mech. Eng. 233 (4), 824–838.

Lv, L., Shao, W., Tang, J., Zhao, J., Kontziampasis, D., Liang, Z., 2025. Surface hardening analysis in shot peening of AISI 9310 gear steel driven by grain and dislocation coupling effects. Materials Characterization 2025, 114788. https://doi.org/10.1016/j.matchar.2025.114788.

Merchant, M.E., 1945. Mechanics of the metal cutting process. J. Appl. Phys. 16, 267–279. https://doi.org/10.1115/1.4009380.

Nategh, M.J., Razavi, H., Abdullah, A., 2012. Analytical modeling and experimental investigation of ultrasonic-vibration assisted oblique turning, part I: kinematics analysis. Int. J. Mech. Sci. 63, 1–11. https://doi.org/10.1016/j.ijmecsci.2012.06.007.

Ni, C., Zhu, L., Liu, C., Yang, Z., 2018. Analytical modeling of tool-workpiece contact rate and experimental study in ultrasonic vibration-assisted milling of Ti-6Al-4V. Int. J. Mech. Sci. 142–143, 97–111. https://doi.org/10.1016/j.ijmecsci.2018.04.037.

Ni, C., Zhu, L., Yang, Z., 2019. Comparative investigation of tool wear mechanism and corresponding machined surface characterization in feed-direction ultrasonic vibration assisted milling of Ti6Al4V from dynamic view. Wear 436–437, 1–17. https://doi.org/10.1016/j.wear.2019.203006, 203006.

Patil, S., Joshi, S., Tewari, A., Joshi, S.S., 2014. Modeling and simulation of effect of ultrasonic vibration on machining of Ti6Al4V. Ultrasonics 94, 694–705. https://doi.org/10.1016/j.ultras.2013.09.010.

Roshchupkin, V.V., Semashko, N.A., Lanovenko, E.V., 2001. Acoustic Properties of VT20 Titanium Alloy in the Temperature Range from 300 to 1300 K. High Temperature 39 (4), 634–636.

Shi, Z., Chen, C., Gong, Y., Yang, Z., Bao, Y., 2024. Sustainable and environmentally friendly longitudinal-torsional ultrasonic cryogenic cooling drilling system. J. Clean. Prod. 468, 143001. https://doi.org/10.1016/j.jclepro.2024.143001.

Skelton, R.C., 1969. Effect of ultrasonic vibration on the turning process. Int. J. Mach. Tool Des. Res. 9, 363–374. https://doi.org/10.1016/0020-7357(69)90020-1.

Sun, Z., Liu, Y., Geng, D., Zhang, D., Ying, E., Liu, R., Jiang, X., 2025. Cutting performance and surface integrity during rotary ultrasonic elliptical milling of cast Ni-based superalloy. Journal of Materials Research and Technology 35, 980–994. https://doi.org/10.1016/j.jmrt.2025.01.079.

Tan, R., Zhao, X., Guo, S., Zou, X., He, Y., Geng, Y., Hu, Z., Sun, T., 2020. Sustainable production of dry-ultra-precision machining of Ti-6Al-4V alloy using PCD tool under ultrasonic elliptical vibration assisted cutting. J. Clean. Prod. 248, 119254. https://doi.org/10.1016/j.jclepro.2019.119254.

Toropov, A., Ko, S.L., 2007. Prediction of shear angle for continuous orthogonal cutting using thermo-mechanical constants of work material and cutting conditions. J. Mater. Process. Technol. 182, 167–173. https://doi.org/10.1016/j.jmatprotec.2006.07.027.

Verma, G.C., Pandey, P.M., Dixit, U.S., 2018. Modeling of static machining force in axial ultrasonic-vibration assisted milling considering acoustic softening. Int. J. Mech. Sci. 136, 1–16. https://doi.org/10.1016/j.ijmecsci.2017.11.048.

Vyas, A., Shaw, M.C., 1999. Mechanics of saw-tooth chip formation in metal cutting. J. Manuf. Sci. E-T. ASME 121, 163–171. https://doi.org/10.1115/1.2831200.

Wallace, P.W., Boothroyd, G., 1964. Tool forces and tool-chip friction in orthogonal machining. J. Mech. Eng. Sci. 6, 74–87. https://doi.org/10.1243/JMES_JOUR_1964_006_013_02.

Wang, L.J., Zhao, J., 1987. Influence on surface roughness in turning with ultrasonic vibration tool. Int. J. Mach. Tool Des. Res. 27 (2), 181–190. https://doi.org/10.1016/S0890-6955(87)80049-4.

Wang, Y., Liang, Z., Zhao, W., Wang, X., Wang, H., 2020. Effect of ultrasonic elliptical vibration assistance on the surface layer defect of M-plane sapphire in microcutting. Mater. Des. 192, 10875. https://doi.org/10.1016/j.matdes.2020.108755.

Wright, P.K., 1981. Frictional interactions in machining: comparisons between transparent sapphire and steel cutting tools. Met. Technol. 8 (4), l50–l160. https://jglobal.jst.go.jp/en/detail?JGLOBAL_ID=200902087626586244.

Wright, P.K., Home, J.G., Tabor, D., 1979. Boundary conditions at the chip-tool interface in machining: comparisons between seizure and sliding friction. Wear 54, 371–390. https://doi.org/10.1016/0043-1648(79)90128-5.

Yao, G., Zhang, D., Geng, D., Wang, L., 2021. Novel ultrasonic vibration-assisted electrosurgical cutting system for minimizing tissue adhesion and thermal injury. Mater. Des. 201, 109528. https://doi.org/10.1016/j.matdes.2021.109528.

Zarchi, M., Razfar, M., Abdullah, A., 2013. Influence of ultrasonic vibrations on side milling of AISI 420 stainless steel. Int. J. Adv. Manuf. Technol. 66, 83–89. https://link.springer.com/article/10.1007/s00170-012-4307-9.

Zhang, W.X., Zhang, J.J., Wang, Z.F., 2024. Promoted grain refinement in tool-chip interface during ultrasonic elliptical vibration-assisted cutting of polycrystalline copper. Int. J. Adv. Manuf. Technol. 134 (7–8), 3925–3936. https://link.springer.com/article/10.1007/s00170-024-14341-w.

Zhang, X., Sui, H., Zhang, D., Jiang, X., 2018. Study on the separation effect of high-speed ultrasonic vibration cutting. Ultrasonics 87, 166–181. https://doi.org/10.1016/j.ultras.2018.02.016.

Zorev, N.N., 1963. Interrelationship between shear processes occurring along tool face on shear plane in metal cutting. Int. Res. Prod. Eng. ASME. 1, 42–49. https://doi.org/10.1016/j.procir.2021.09.069.

Zhu, J., Shao, W., Huang, W., Tang, J., Jiang, T., Shen, X., 2025. Mechanical response of carbon ion implanted ferrite via atomic simulations. International Journal of Mechanical Sciences 285, 109837. https://doi.org/10.1016/j.ijmecsci.2024.109837.